CHEMISTRY
A EUROPEAN JOURNAL

DOI: 10.1002/chem.200600460

Probing Structural Effects on Replication Efficiency through Comparative Analyses of Families of Potential Self-Replicators

Eleftherios Kassianidis, Russell J. Pearson, and Douglas Philp*[a]

Abstract: A formidable synthetic apparatus for the creation of nanoscale molecular structures and supramolecular assemblies through molecular structures can potentially be created from systems that are capable of parallel automultiplication (self-replication). In order to achieve this goal, a detailed understanding of the relationship between molecular structure and replication efficiency is necessary. Diastereoisomeric templates that are capable of specific and simultaneous autocatalysis have been synthesised. A systematic experimental and theoretical evaluation of their behaviour and that of structurally-related systems reveals the key determinants that dictate the emergence of self-replicative function and defines the structural space within which this behaviour is observed.

Keywords: kinetics · molecular recognition · recognition-mediated reactions · self-replication · supramolecular chemistry

Introduction

The formulation of a generally-applicable conceptual framework that would facilitate the rapid development and deployment of self-replicating[1] molecular architectures[2] could potentially revolutionise materials fabrication at the nanometer scale. One can envision that the emergence of such a self-replication protocol would deliver a formidable, self-instructed synthetic apparatus[3] functioning in an economical and environmentally benign fashion. In order to achieve this ambitious goal, a fundamental understanding of recognition-mediated processes that allow molecules to template their own formation is an important requirement. Within this broad objective, the development of efficient protocols which allow self-replication and genotypic (Darwinian) evolution[4] within supramolecular assemblies is essential. A clear understanding of the nature of the recognition-mediated processes which allow molecules to template their own formation is therefore an important requirement. We have become interested in the factors that govern the choice of reaction pathway adopted by systems whose reactivity is mediated[5] by recognition processes. Ultimately, we wish to exploit replicating systems in the construction[6] and amplification[7] of large molecular and supramolecular assemblies.

In the last 15 years, several examples[8] of self-replicating systems capable of templating and catalysing their own synthesis have appeared[9] in the chemical literature. Almost all of the examples of synthetic self-replicators reported in this period are based on the minimal model[10] shown in Figure 1. This minimal model of self-replication contains three distinct reaction channels. The first is the uncatalysed bimolecular reaction between reagents A and B to afford the template T. A key requirement of the model is that A and B bear complementary recognition sites such that A and B can associate with each other to form a binary complex, [A·B]. The presence of this complex opens a second reaction channel—the binary complex channel—in which A and B are preorganised[11] with respect to each other and the reaction between them is pseudo-intramolecular. The product of this reaction channel forms a closed template $T_{inactive}$ in which the recognition used to assemble the binary complex lives on in the template, thus, although rate acceleration is achieved[5] by this mechanism, this template is inert catalytically.

The third reaction channel available to the system is the autocatalytic[12] cycle. In this channel, A and B bind reversibly to the open template T to form a catalytic ternary complex [A·B·T]. In a manner similar to the [A·B] complex, the reaction between A and B is also rendered pseudo-intramolecular. Bond formation occurs between A and B to give the product duplex [T·T], which then dissociates to return two

[a] Dr. E. Kassianidis, Dr. R. J. Pearson, Dr. D. Philp
Centre for Biomolecular Sciences, School of Chemistry
University of St Andrews, North Haugh, St Andrews KY16 9ST (UK)
Fax: (+44) 1334-463-808
E-mail: d.philp@st-andrews.ac.uk

Supporting information for this article is available on the WWW under http://www.chemeurj.org/ or from the author.

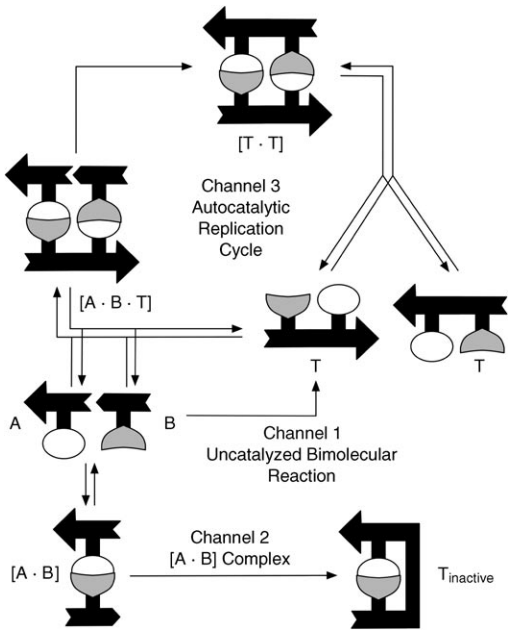

Figure 1. Minimal model of self-replication. Reagents A and B can react through three pathways. Channel 1: uncatalysed bimolecular reaction. Channel 2: Recognition-mediated pseudounimolecular pathway mediated by a binary complex [A·B]. Channel 3: Recognition-mediated pseudounimolecular autocatalytic cycle mediated by a ternary complex [A·B·T].

molecules of T to the start of the autocatalytic cycle. Thus, assuming the open template T presents its recognition sites in the correct orientation, it can act as a template for its own formation, transmitting molecular information through the formation of identical copies of itself. Our initial forays[13] in the field of molecular self-replication focused on the utilisation of bifunctional precursor subunits which incorporate mutually complementary recognition elements (essential for reversible, intermolecular assembly) and reactive functionalities (essential for the irreversible construction of scaffolds). These features are combined to engineer linear self-complementary platforms capable of autocatalytic self-propagation through the mechanism illustrated in Figure 1.

In our overall strategy, the development of replicating systems that can operate independently or in concert within the same reaction mixture is of great significance. We identified the Diels–Alder reaction between alkylfurans and maleimides as a particularly suitable platform[14] upon which to conduct the search for systems that display this important property. This reaction[15] affords two products—the *endo* cycloadduct and the *exo* cycloadduct—which differ in the relative stereochemistry at the 6–5 ring junction and these two cycloadducts have markedly different geometries. The reaction proceeds under mild conditions without the need for external reagents, making it ideal for study by NMR methods. Our approach to studying molecular replication involves rigorous experimental and theoretical analyses of systems that are intimately related in a constitutional sense. From these studies we wish to pinpoint the key determinants that enable: i) the emergence of self-replicative function, ii) the efficiency of self-replication, iii) the suppression (or ideally eradication) of the binary reactive complex route in favour of the self-replicative route, iv) the enhancement of diastereoselectivity (translation of stereochemical information from parent template to offspring), and v) the social behaviour of self-replicating species (i.e., emergence of synergistic or cross-catalytic behaviour, autocratic or independent/non-cooperative networks). Having established these factors, we must incorporate our conclusions to current methodologies, thus expanding the scope and applicability of the self-replication technology.

In this work, we describe two systems which each contain a pair of diastereoisomeric replicators which are capable of specific autocatalysis without concomitant cross-catalysis. This behaviour is rationalised and explained using experimental and computational methods in terms of the different recognition-mediated reaction pathways—facilitated by the amidopicoline–carboxylic acid[16] recognition motif—which predominate in these templates. Additionally, we demonstrate, through programmed variation of the constitution of the components of the recognition-mediated reactions, that the structural window within which this behaviour is observed is rather narrow.

Results and Discussion

In order to investigate the relationship between structure and function in minimal self-replicating systems, it is necessary to examine the role that systematic structural variation plays in determining the recognition-mediated reactivity displayed by a particular system. To this end, we designed and synthesised (Figure 2) furans **1** through **4** and maleimides **5a** and **6a**. All dienes contain a carboxylic acid recognition site which can associate in non-polar solvents—through two hydrogen bonds (Figure 2)—with the amidopyridine recognition site located on the dienophiles. Reaction of the diene with the dienophile gives rise to two diastereoisomeric cycloadducts, *endo* and *exo*. The structural variation inherent in this system affords three sites of variability—the number of methylene spacers between the recognition sites and the reactive sites (*m* and *n* in Figure 2), and the location of the spacer on the diene (furan substitution in Figure 2).

Therefore, pairwise combination of each of the dienes with each of the dienophiles gives rise to eight distinct systems—labelled system I through VIII in Figure 2—with the capacity for recognition-mediated reactivity and therefore, potentially, replication. It is noteworthy that the diastereoisomeric pairs of e*ndo* and *exo* cycloadducts (produced from common precursors, for example, **1** and **5a**) possess dissimilar configurational and geometrical features. Consequently, although identical, peripherally extending recognition elements are affixed to identical positions on the tricyclic core of respective *endo* and *exo* cycloadducts through identical alkyl spacer units, these recognition sites explore disparate conformational landscapes. This difference is significant, since the three-dimensional structure and folding of each di-

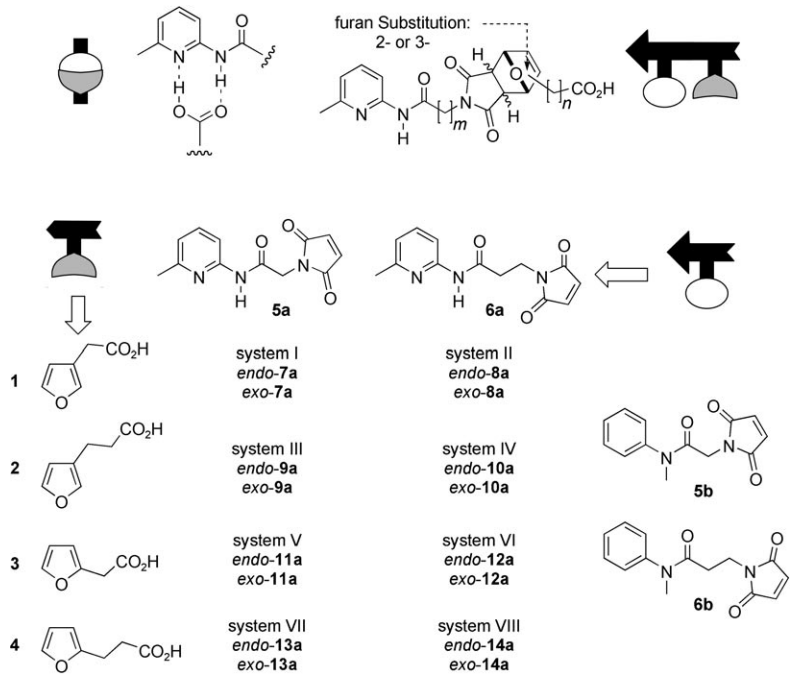

Figure 2. Design of self-replicating templates. The cartoons relate the chemical structures to the schematic mechanism shown in Figure 1.

astereoisomer determines its self-templating capacity. Additionally, we introduced variation in the position of substitution on the furan ring since we expected there to be behavioural and mechanistic discrepancies between constitutional isomers such as *exo*-**8a** and *exo*-**12a**.

In any assessment of reactivity, suitable control compounds are required. We therefore designed and synthesised maleimides **5b** and **6b** as suitable controls for systems I through VIII since they lack the appropriate amidopyridine recognition site whilst retaining the other structural and electronic features of **5a** and **6a**. In the discussion which follows, any compound with the designator **b** refers to a control compound and any compound with the designator **a** refers to a compound with the capacity for recognition. All compounds were synthesised by standard methods—details are given in the Experimental Section and the Supporting Information.

Kinetic investigations: Our standard kinetic analysis[12] of each of the systems I through VIII, employed four diagnostic experiments—detailed below—performed on each system at a range of temperatures. Computational kinetic simulations and electronic structure calculations of reaction transition states complemented these experiments. All kinetic experiments reported in detail here were undertaken in $CDCl_3$ at 35 °C (systems I–VI) or 45 °C (systems VII and VIII).

Reaction mixtures were prepared and assayed at fixed intervals by 500 MHz ^{1}H NMR spectroscopy, and reaction progress was assessed by monitoring the disappearance or appearance of the appropriate resonances in the region δ 6.80 to 6.99 (maleimide) or δ 5.20 to 5.60 (cycloadducts) as a function of time. Product concentrations were calculated from the ^{1}H NMR spectroscopic data by deconvolution methods. All kinetics experiments were performed under thermostatically controlled conditions ($\pm$0.1 °C).

We did not observe decomposition or the formation of unexpected side products in any of the kinetics experiments performed. Retro Diels–Alder reactions[17] involving furans and maleimides[18] are well documented and known to occur rapidly at elevated temperatures ($T > 100$ °C). In the temperature range and timescale of our investigations, complications resulting from extensive interconversion of *endo* and *exo* cycloadducts did not arise. However, minor effects from this phenomenon were taken into account in our kinetic modelling studies (see Supporting Information). In summary, experimental time courses for the formation of cycloadducts *endo*-**7a** through **14a** and *exo*-**7a** through **14a** were obtained using reaction mixtures containing the appropriate dienes and dienophiles ([diene] = [dienophile] = 25.0 mM) in $CDCl_3$.

Measures of the kinetic parameters and diastereoselectivities of the non-recognition-mediated mode of reactivity between dienes and dienophiles were obtained through kinetic experiments in which the original dienophiles **5a** or **6a** were replaced by non-associating maleimides (NAMs) **5b** or **6b**, respectively. Starting concentrations of [diene] = [NAM] = 25.0 mM were employed in all cases. These model reactions served as excellent reference points, enabling direct comparisons of catalysed (recognition-mediated/pseudounimolecular) and uncatalysed (non recognition-mediated/bimolecular) pathways and, ultimately, permitting quantification of self-replicative proficiency.

Competitive inhibition experiments involved the addition of 4.0 equivalents of benzoic acid (BA) to reaction mixtures consisting of diene and dienophile building blocks ([diene] = [dienophile] = 25.0 mM, [BA] = 100.0 mM). These experiments assisted qualitative evaluation of the significance of hydrogen bonding to the observed rate accelerations. Benzoic acid obstructs the assembly of the catalytically crucial ensembles [diene•dienophile•adduct], by competitively occupying amidopicoline recognition sites of dienophiles and cycloadducts. Hence, reactions that are genuinely orchestrated by hydrogen bonding should display reductions in reaction rate in the presence of benzoic acid.

Lastly, the self-replicative/autocatalytic capacity of the Diels–Alder cycloadducts was examined by incorporating

catalytic amounts of the prefabricated cycloadducts ($[adduct]_{initial}=1.2$–3.5 mM) to the reaction mixtures containing stoichiometric concentrations of the constituent fragments ([diene]=[dienophile]=25.0 mM): It was envisaged that substantial increases in reaction velocity—proportional to the increase of concentration of catalytically active species (in comparison to reactions where $[adduct]_{initial}=0$)—should be observed in cases where adducts exhibited self-replicative function. On the contrary, the injection of sub-stoichiometric amounts of self-complementary scaffolds bearing recognition sites associated in an intramolecular fashion ($T_{inactive}$ in Figure 1), should not result in increases in reaction velocity. In effect, presynthesised templates acted as mechanistic probes, invaluable for mapping out predominant reactive pathways: self-replication (or ternary complex) pathway in the first instance and binary complex pathway in the second instance. Nevertheless, in the majority of situations, mathematical treatment of experimental data pointed to some concurrent operation of all three reaction channels.

The combination of these four experiments—performed on each system in turn—allows an initial assessment of the presence (or absence) of a dominant recognition-mediated reaction channel in a given situation. Finer-grained analysis of the behaviour of the systems becomes possible after the simulation and fitting of the kinetic data to the appropriate reaction model and the careful analysis of the best-fit kinetic parameters thus obtained for each system.

As a result of the sheer volume of data generated within this study, we will focus in depth only on systems displaying unusually interesting characteristics.

System II: In this system, the diene has a single methylene spacer between the recognition site and the furan ring and there are two methylenes connecting the dienophile to the amidopyridine recognition site. The control reaction between **1** and **6b** reveals that, after 16 h at 35 °C in $CDCl_3$ where [**1**]=[**6b**]=25.0 mM, the total conversion was 19% and the *endo*-**8b**:*exo*-**8b** ratio was 1.6:1. Analysis of this data by kinetic simulation and fitting afforded the initial rates of formation of *endo*-**8b** and *exo*-**8b** as $r(endo\text{-}\mathbf{8b})=4.14\times10^{-5}$ mM s^{-1} and $r(exo\text{-}\mathbf{8b})=2.66\times10^{-5}$ mM s^{-1}, respectively (Figure 3).

When the control dienophile **6b** was replaced by the recognition-capable dienophile **6a**, the initial rates of formation of cycloadducts *endo*-**8a** and *exo*-**8a** increased significantly. In the reaction between **1** and **6a** ([**1**]=[**6a**]=25.0 mM), the initial rates of reaction increased to $r(endo\text{-}\mathbf{8a})=9.79\times10^{-5}$ mM s^{-1} (2.4-fold increase) and $r(exo\text{-}\mathbf{8a})=7.68\times10^{-5}$ mM s^{-1} (2.9-fold increase). After 16 h, in the presence of recognition the total conversion was now 41%. A minor change in the diastereoselectivity was also observed (*endo*-**8b**:*exo*-**8b**=1.1:1). These observations when combined, insinuate the presence of catalytic forces, possibly emanating from the assembly of ternary aggregates [**1**·**6a**·*endo*-**8a**], [**1**·**6a**·*exo*-**8a**] or the binary aggregate [**1**·**6a**].

The introduction of benzoic acid as competitive inhibitor ([**1**]=[**6a**]=25.0 mM, [BA]=100.0 mM) resulted in reduction

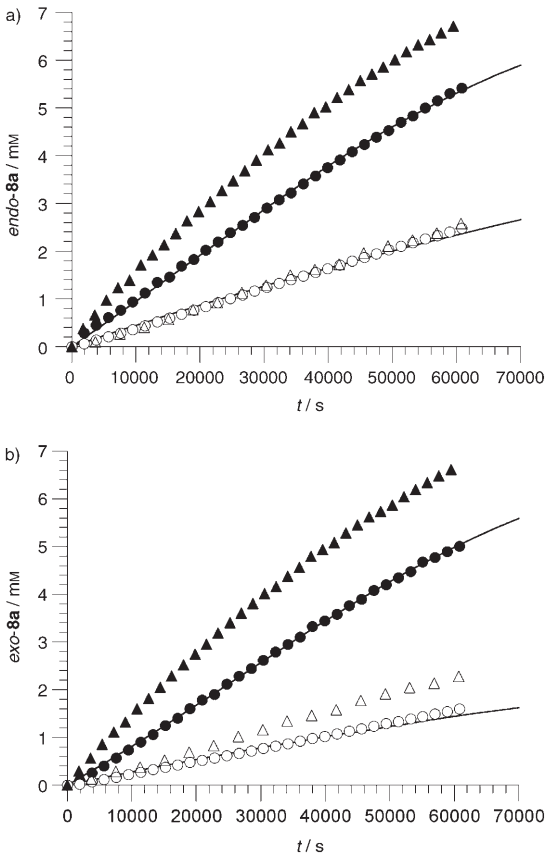

Figure 3. Rate profiles at 35 °C in $CDCl_3$, for the formation of a) *endo*-**8a** or *endo*-**8b** and b) *exo*-**8a** or *exo*-**8b** from building blocks **1** and **6a** and **1** and **6b**, respectively. Starting concentrations of diene and dienophile were 25 mM. ●: Reaction between **1** and **6a** (Recognition-mediated reaction). ○: Reaction between **1** and **6b** (Bimolecular reaction). △: Reaction between **1** and **6a** in the presence of 4 equiv $PhCO_2H$ (competitive inhibitor). ▲: Reaction between **1** and **6a** in the presence of preformed *endo*-**8a** (10 mol%) or *exo*-**8a** (8 mol%). Solid lines represent the best fit of the experimental data to the appropriate kinetic model using the SimFit[19] package. See Supporting Information for further details of the kinetic models used.

of the initial rates of cycloadducts formation back to levels almost identical to those observed in the control (bimolecular) reaction: $r(endo\text{-}\mathbf{8a})=4.32\times10^{-5}$ mM s^{-1} and $r(exo\text{-}\mathbf{8a})=3.85\times10^{-5}$ mM s^{-1}. This observation demonstrates that recognition is pivotal for the emergence of rate acceleration within this system, whilst simultaneously ruling out adventitious general Lewis acid catalysis of the cycloaddition reaction arising from the presence of carboxylic acid moieties that are located on precursor **1** and products *endo*-**8a** and *exo*-**8a.** Although this experiment demonstrates the recognition-mediated nature of the processes forming *endo*-**8a** and *exo*-**8a**, two mechanistic possibilities still exist. Each cycloadduct, *endo*-**8a** and *exo*-**8a**, could function as an isolated self-replicator, autonomously self-propagating in the absence of synergism or inhibition with its diastereoisomer. Alternatively, each diastereoisomer could, in addition to self-replication, participate in the operation of parallel, interdependent subnetworks (hypercycles), sustained by col-

laborative catalysis—where proliferation of *endo*-**8a** is catalysed by itself and by *exo*-**8a** and vice versa.

According to the general protocol described above, the ability of the reaction products (templates) *endo*-**8a** and *exo*-**8a** to synchronously bind their constituent fragments (imposing the propinquity of reactive functionalities and, hence, bringing about increases in reaction velocity) can be evaluated by computing initial rates of generation of *endo*-**8a** and *exo*-**8a** in reactions between **1** and **6a** ([**1**] = [**6a**] = 25.0 mM) in the presence of *endo*-**8a** (2.5 mM) and *exo*-**8a** (2.3 mM). When such template-directed reactions were performed, the expected rate increases were observed—the formation of both *endo*-**8a** and *exo*-**8a** was accelerated, with $r(\textit{endo}\text{-}\mathbf{8a}) = 15.75\times10^{-5}$ mM s^{-1} and $r(\textit{exo}\text{-}\mathbf{8a}) = 14.82\times10^{-5}$ mM s^{-1} corresponding to accelerations of 3.8- and 4.6-fold over the bimolecular control. It was therefore concluded that the production of *endo*-**8a** and *exo*-**8a** was mediated by the ternary complexes [**1**·**6a**·*endo*-**8a**] and [**1**·**6a**·*exo*-**8a**]. In these experiments, marginal increases (in comparison with the reaction between **1** and **6a**) in the fraction of *exo*-**8a** produced (*endo*-**8a**:*exo*-**8a** = 1:1) and total conversion (54%) were also observed. These results suggest that *endo*-**8a** and *exo*-**8a** replicate independently. In other words, *endo*-**8a** is a catalyst for its own formation, but not for the formation of *exo*-**8a** and vice versa. In other words, neither template engages in cross-catalytic behaviour.

The source of this dramatic catalytic selectivity must arise from the location of the recognition elements in space and the congruency of the transition state with the supporting template structure.

In order to probe these effects more deeply, we performed a series of calculations using both molecular mechanics (AMBER* force field) and electronic structure methods (at the B3LYP/6-31G level of theory). We calculated the minimum energy conformations of the isolated templates *endo*-**8a** and *exo*-**8a**, the corresponding homodimeric duplexes [*endo*-**8a**·*endo*-**8a**] and [*exo*-**8a**·*exo*-**8a**] and the heterodimeric duplex [*endo*-**8a**·*exo*-**8a**].

It is evident from an examination of Figure 4 that *endo*-**8a** and *exo*-**8a** are geometrically incongruent. The homodimers [*endo*-**8a**·*endo*-**8a**] and [*exo*-**8a**·*exo*-**8a**] are capable of supporting four hydrogen bonds. However, the heterodimer [*endo*-**8a**·*exo*-**8a**] cannot support more than a single association between an amidopyridine of one template and the carboxylic acid of its diastereoisomer. Therefore, one might expect that the transition states leading to *endo*-**8a** and *exo*-**8a** might also be basically incongruent resulting in the absence of any cross-catalytic capacity in the templates. In order to probe this hypothesis, we calculated the structures of the *exo* transition state docked on the *exo*-**8a** template and the *endo* transition state docked on the *endo*-**8a** template. Additionally, we attempted to dock the diastereomerically mismatched transition states and templates. The results of these calculations are revealing. The diastereomerically-matched transition states are supported elegantly (Figure 5) by the corresponding templates suggesting that these reactions can proceed readily on the matched template. However, it proved impossible to locate plausible transition state structures for the mismatched pairs suggesting that it is not possible for a ternary complex to enter the reaction cross-section leading to a cross-catalytic transition state.

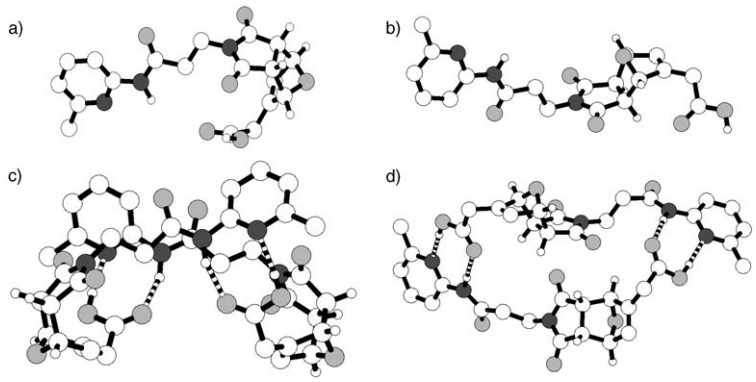

Figure 4. a) Ball-and-stick model of a representative low energy conformation of *endo*-**8a**. b) Ball-and-stick model of a representative low energy conformation of *exo*-**8a**. c) Ball-and-stick model of a representative low energy conformation of [*endo*-**8a**·*endo*-**8a**]. d) Ball-and-stick model of a representative low energy conformation of [*exo*-**8a**·*exo*-**8a**]. All structures were calculated using AMBER* force field. Carbon atoms are coloured white, oxygen atoms are coloured light grey, nitrogen atoms are coloured dark grey. Some hydrogen atoms have been omitted for clarity. Hydrogen bonds are represented by dashed lines.

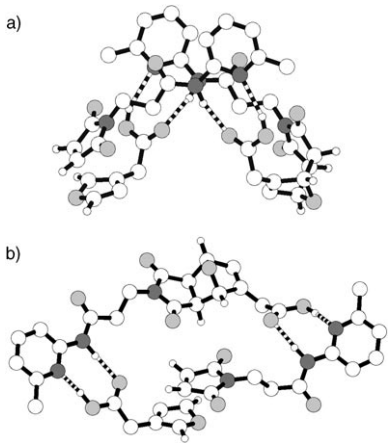

Figure 5. a) Ball-and-stick representation of the calculated (B3LYP/6-31G(d)) transition state for the formation *endo*-**8a** within the [**1**·**6a**·*endo*-**8a**] complex. b) Ball-and-stick representation of the calculated (B3LYP/6-31G(d)) transition state for the formation *exo*-**8a** within the [**1**·**6a**·*exo*-**8a**] complex. Carbon atoms are coloured white, oxygen atoms are coloured light grey, nitrogen atoms are coloured dark grey. Some hydrogen atoms have been omitted for clarity. Hydrogen bonds are represented by dashed lines.

Experimental support for these computational results comes from extensive gradient NOE difference analyses (Figure 6). Equimolar mixtures of *endo*-**8a** and *exo*-**8a** ([*endo*-**8a**] = [*exo*-**8a**] = 10.0 mM) were subjected to analysis by 500 MHz ^{1}H NMR spectroscopy in $CDCl_3$ at 25 °C. These studies were able to establish a number of NOE enhancements which could only arise from the homodimeric structures [*endo*-**8a**•*endo*-**8a**] and [*exo*-**8a**•*exo*-**8a**]. For example, irradiation (Figure 6) at the resonance frequency of H_e, situated upon the *endo*-**8a** scaffold, positive intramolecular NOE values were observed for adjacent protons H_f and positive intermolecular NOE values for H_g, signifying the presence of the homodimer [*endo*-**8a**•*endo*-**8a**]. It is noteworthy that this observed NOE signal is consistent with the structure of the [*endo*-**8a**•*endo*-**8a**] duplex shown in Figure 4. No NOE evidence emerged which supported the presence of significant quantities of the heterodimeric structure [*endo*-**8a**•*exo*-**8a**] in solution under these conditions.

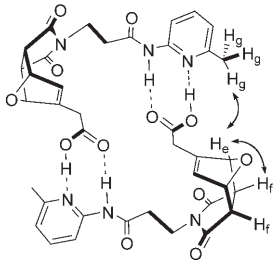

Figure 6. Inter- and intramolecular NOE within the homodimeric aggregate [*endo*-**8a**•*endo*-**8a**] observed in $CDCl_3$ at 35 °C using 500 MHz ^{1}H NMR spectroscopy.

Elucidation of the mechanistic subtleties of recognition-mediated processes is predicated upon the construction of reaction models that can faithfully reproduce experimental time courses by numerical simulation. In this way, we can maximise the amount of information we can extract from our kinetic experiments by determining more accurately the relative contributions of the various reaction pathways. In the case of this system, we postulated that species *endo*-**8a** and *exo*-**8a** are formed through the concurrent operation of the three channels shown in Figure 1 and that the replication channel for each diastereoisomer (*exo*-**8a** and *endo*-**8a**) operate in a mutually-exclusive manner. Details of the reaction model used are given in the Supporting Information. Fitting of this reaction model to the concentration versus time data obtained for this system (solid lines in Figure 3) enabled the calculation of rate constants and, hence, kinetic[20] and thermodynamic[21] effective molarity[22] values (denoted as k_{EM} and t_{EM}, respectively), characteristic of the binary reactive complex channel and the templated (ternary complex) channel (Table 1).

The results clearly demonstrate that, in this system, the efficiency of the binary complex channel is rather low—uniformly an order of magnitude less than the autocatalytic channel. The kinetic effective molarities of close to 1 M for the two diastereoisomeric templates indicate that the level of transition state stabilisation present in the ternary complexes is relatively low—of a similar magnitude to the free energy of binding of the components of the replicator. This result is not unsurprising given the relative flexibility of the templates and the resistance of cycloaddition reaction to acceleration by intramolecularisation. The k_{EM} for *exo*-**8a** is significantly higher than that for *endo*-**8a** and this observation probably reflects a better fit of the transition state to the template (Figure 5). The most interesting aspect of this system is the presence of two independent autocatalytic channels that operate independently in such a structurally simple system.

Table 1. Calculated kinetic and thermodynamic effective molarity values associated with formation of *endo*-**8a** and *exo*-**8a** through the operation of the self-replicative and the binary reactive complex pathways at 35 °C in $CDCl_3$.

Reaction pathway (35 °C)	k_{EM}(*endo*-**8a**) [mM]	t_{EM}(*endo*-**8a**) [mM]	k_{EM}(*exo*-**8a**) [mM]	t_{EM}(*exo*-**8a**) [mM]
self-replication	663	289	1100	367
binary reactive complex	70	31	96	37

System III: The diastereoisomeric pair of templates *endo*-**9a**/*exo*-**9a** are constitutional isomers of *endo*-**8a**/*exo*-**8a**. The length of the spacers that connect the recognition sites to the reactive sites differentiates the two pairs of cycloadducts. In system II, the carboxylic acid is connected to the diene by a single CH_2 and the amidopyridine is connected to the maleimide by a CH_2CH_2 group. In system III, the placement of these spacer groups is reversed—the carboxylic acid is connected to the diene by a CH_2CH_2 group and the amidopyridine is connected to the maleimide by a single CH_2. By examining the behaviour of system III, we hoped to gain insight into the resilience of the replicating behaviour of system II to small structural changes.

Once again, kinetic experiments (Figure 7) were performed at 35 °C in $CDCl_3$. In the control reaction, the Diels–Alder cycloaddition between **2** and **5b** ([**2**] = [**5b**] = 25.0 mM), afforded *endo*-**9b** and *exo*-**9b** with respective initial velocities of r(*endo*-**9b**) = 6.73×10^{-5} mM s^{-1} and r(*exo*-**9b**) = 3.85×10^{-5} mM s^{-1} (Table 2). In the recognition-mediat-

Table 2. Measured initial rates of formation of *endo*-**9** and *exo*-**9** at 35 °C in $CDCl_3$. Relative rates are calculated assuming the reaction between **2** and **5b** has a rate of 1 mM s^{-1}.

Reaction (35 °C/$CDCl_3$)	r(*endo*-**9**) ($\times 10^{-5}$) [mM s^{-1}]	Relative rate (*endo*-**9**)	r(*exo*-**9**) ($\times 10^{-5}$) [mM s^{-1}]	Relative rate (*exo*-**9**)	Total conversion % (in 16 h)
2 + **5b**	6.73	1.0	3.85	1.0	25
2 + **5a**	11.50	1.7	8.27	2.2	38
2 + **5a** + BA	10.57	1.5	5.24	1.4	30
2 + **5a** + template	15.80	2.4	11.40	3.0	44

ed reaction between carboxylic acid **2** and **5a** ([**2**]=[**5a**]=25.0 mM) rate enhancements of 1.7-fold for *endo*-**9a** and 2.2-fold for *exo*-**9a** are observed.

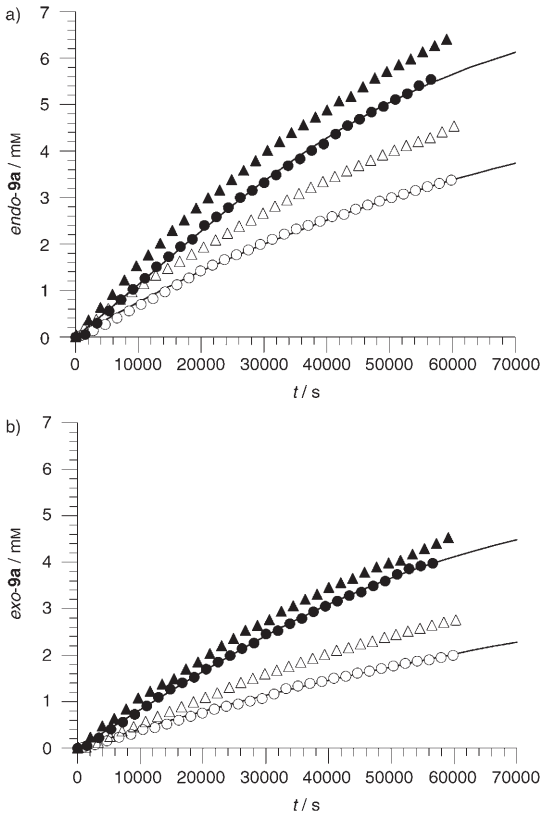

Figure 7. Rate profiles, at 35 °C in $CDCl_3$, for the formation of a) *endo*-**9a** or *endo*-**9b** and b) *exo*-**9a** or *exo*-**9b** from building blocks **2** and **5a** and **2** and **5b**, respectively. Starting concentrations of diene and dienophile were 25 mM. ●: Reaction between **2** and **5a** (recognition-mediated reaction). ○: Reaction between **2** and **5b** (bimolecular reaction). △: Reaction between **2** and **5a** in the presence of 4 equiv $PhCO_2H$ (competitive inhibitor). ▲: Reaction between **2** and **5a** in the presence of preformed *endo*-**9a** (10 mol%) or *exo*-**9a** (7 mol%). Solid lines represent the best fit of the experimental data to the appropriate kinetic model using the SimFit[19] package. See Supporting Information for further details of the kinetic models used.

The addition of the competitive inhibitor benzoic acid ([**2**]=[**5a**]=25.0 mM, [BA]=100.0 mM) induced a reduction of the initial velocity for the formation of *endo*-**9a** and *exo*-**9a** (Table 2), thus providing firm evidence of the connection between hydrogen bonding and rate acceleration.

Finally, the addition of 2.5 mM of *endo*-**9a** and 1.7 mM of *exo*-**9a** into reaction mixtures containing equimolar concentrations of **2** and **5a** ([**2**]=[**5a**]=25.0 mM), resulted in measured initial rates of $r(endo\text{-}\mathbf{9a})=15.80\times10^{-5}$ mM s^{-1} and $r(exo\text{-}\mathbf{9a})=11.40\times10^{-5}$ mM s^{-1} corresponding to increases of 2.4- and 3-fold in comparison to the bimolecular reaction (Table 4). The latter observation demonstrates the ability of both *endo*-**9a** and *exo*-**9a** to template their own formation. As in the case of system II, cross-catalysis between the diastereoisomeric replicators is precluded by the geometric incongruence of the *endo* and *exo* cycloadducts.

As before we attempted to reproduce the experimental rate profiles through kinetic simulation and fitting. Fitting of the appropriate reaction model to the concentration/time data obtained for this system (solid lines in Figure 7) enabled the calculation of rate constants and, hence, kinetic and thermodynamic effective molarities (denoted as k_{EM} and t_{EM}, respectively), characteristic of the binary reactive complex and the autocatalytic reaction channels (Table 3).

Table 3. Calculated kinetic and thermodynamic effective molarity values associated with formation of *endo*-**9a** and *exo*-**9a** through the operation of the self-replicative and the binary reactive complex pathways at 35 °C in $CDCl_3$.

Reaction pathway (35 °C)	k_{EM}(*endo*-**9a**) [mM]	t_{EM}(*endo*-**9a**) [mM]	k_{EM}(*exo*-**9a**) [mM]	t_{EM}(*exo*-**9a**) [mM]
self-replication	475	799	719	78
binary reactive complex	46	216	65	16

Once again, the binary complex pathway is suppressed effectively. Templates *endo*-**9a** and *exo*-**9a** participate in independent self-replicating circuits, the maintenance of which is reliant upon the capacity of *endo*-**9a** and *exo*-**9a**—exhibiting dissimilar geometrical features—to independently intercept their precursor fragments **2** and **5a** on their respective recognition surfaces. As before, the kinetic effective molarities of below 1 M for the two diastereoisomeric templates indicate that the level of transition state stabilisation present in the ternary complexes is relatively low—slightly less than the stabilisation of the system through formation of the appropriate ternary complex. Given that the total number of rotors is identical to system II, this result is not unsurprising. The k_{EM} for *exo*-**9a** is significantly higher than that for *endo*-**9a** and this observation once again probably reflects a better fit of the transition state to the template. It is pleasing to note that, in contrast to other replicating systems studied[23] in our laboratory, the systems reported here are resistant to disruption caused by the reversal of spacer location.

Despite the broad similarity in behaviour between systems II and III more detailed comparisons of the results reveal subtle, but important differences. The effective molarities determined for the *endo* templates at 35 °C suggest that the role of recognition is somewhat different in *endo*-**8a** and *endo*-**9a**. Whilst k_{EM}(*endo*-**8a**) > t_{EM}(*endo*-**8a**) suggesting that the major role of recognition is transition state stabilisation, k_{EM}(*endo*-**9a**) < t_{EM}(*endo*-**9a**), suggesting that the major role of recognition is product ground state stabilisation. By contrast, both *exo*-**8a** and *exo*-**9a** appear to operate through transition-state stabilisation with *exo*-**8a** achieving a slightly higher effective molarity. These distinctions between the two systems are clearly a result of minor structural differences in the templates and coconformational divergences in the ternary complexes. However, the exact origins of these differences have not proven amenable to elucidation by computational methods.

System IV: The diastereoisomeric pair *endo*-**10a** and *exo*-**10a** has an additional methylene rotor when compared to either system II or III. In our previous studies, the addition of a methylene rotor to a system that operated predominantly through a replicating pathway was to redirect the reaction through the binary complex. In order to test this hypothesis, we performed the appropriate kinetic experiments at 35 °C in $CDCl_3$. The results of these experiments, which were conducted in a manner analogous to that described above, are given in Figure 8 and Table 4.

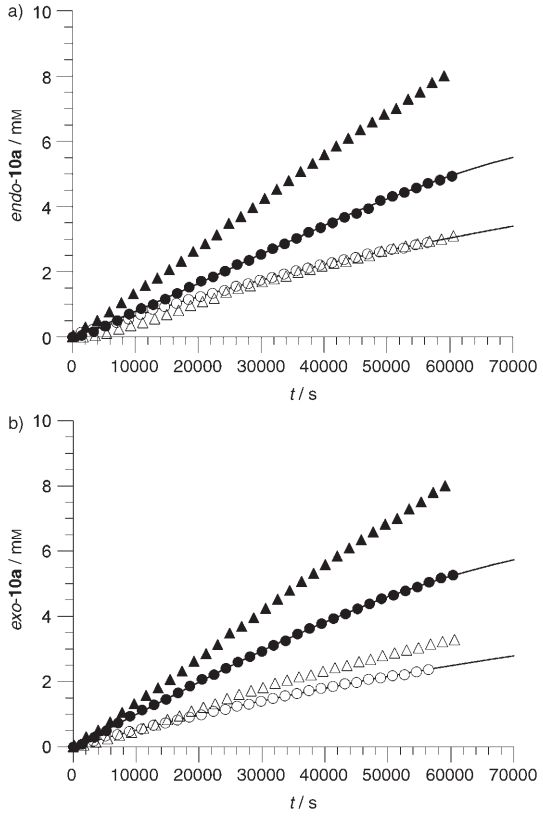

Figure 8. Rate profiles, at 35 °C in $CDCl_3$, for the formation of a) *endo*-**10a** or *endo*-**10b** and b) *exo*-**10a** or *exo*-**10b** from building blocks **2** and **6a** and **2** and **6b**, respectively. Starting concentrations of diene and dienophile were 25 mM. ●: Reaction between **2** and **6a** (recognition-mediated reaction). ○: Reaction between **2** and **6b** (bimolecular reaction). △: Reaction between **2** and **6a** in the presence of 4 equiv $PhCO_2H$ (competitive inhibitor). ▲: Reaction between **2** and **6a** in the presence of preformed *endo*-**6a** (10 mol %) or *exo*-**6a** (8 mol %). Solid lines represent the best fit of the experimental data to the appropriate kinetic model using the SimFit[19] package. See Supporting Information for further details of the kinetic models used.

Further rationalisation of the experimental results was assisted by calculation of effective molarities for the pathways operating in system IV (Table 5).

Surprisingly, interposing an additional rotor into the system does not have the predicted effect. Although the effective molarity values for system IV are lower than the other two systems discussed so far, the predominant pathway is still self-replication. The origins of the observed rate

Table 4. Measured initial rates of formation of *endo*-**10** and *exo*-**10** at 35 °C in $CDCl_3$. Relative rates are calculated assuming the reaction between **2** and **6b** has a rate of 1 mM s^{-1}

Reaction (35 °C/ $CDCl_3$)	r(*endo*-**10**) ($\times 10^{-5}$) [mM s^{-1}]	Relative rate (*endo*-**10**)	r(*exo*-**10**) ($\times 10^{-5}$) [mM s^{-1}]	Relative rate (*exo*-**10**)	Total conversion % (in 16 h)
2 + **6b**	6.04	1.0	5.09	1.0	22
2 + **6a**	8.32	1.4	10.68	2.1	41
2 + **6a** + BA	4.21	0.7	5.15	1.0	25
2 + **6a** + template	13.49	2.3	13.90	2.7	63

Table 5. Calculated kinetic and thermodynamic effective molarity values associated with formation of *endo*-**10a** and *exo*-**10a** through the operation of the self-replicative and the binary reactive complex pathways at 35 °C in $CDCl_3$.

Reaction pathway (35 °C)	k_{EM}(*endo*-**10a**) [mM]	t_{EM}(*endo*-**10a**) [mM]	k_{EM}(*exo*-**10a**) [mM]	t_{EM}(*exo*-**10a**) [mM]
self-replication	536	588	448	75
binary reactive complex	36	43	65	63

enhancements in *endo*-**10a** and *exo*-**10a** are, once again, similar to those observed in systems II and III. In this case, k_{EM}(*endo*-**10a**) $\approx t_{EM}$(*endo*-**10a**) suggesting that both transition state stabilisation and product ground state stabilisation play some role. By contrast, k_{EM}(*exo*-**10a**) $\gg t_{EM}$(*exo*-**10a**) suggesting that transition state stabilisation is dominant. However, since k_{EM}(*exo*-**10a**) < 1 M, it would appear that the transition state stabilisation is less than the ground state stabilisation of the system caused by assembly of **2** and **6a** on the *exo*-**10a** template.

System I: In previous work, we noted[23] that the system with the shortest spacer combination is usually the most efficient replicator. In kinetic experiments performed on system I at 15, 25 and 35 °C in $CDCl_3$, only marginal differences were noted between initial rates of the bimolecular control reactions and recognition-mediated processes. These results suggest that the limited conformational freedom present in this system precludes reaction through either the binary complex route or the self-replication cycle.

Given the apparent resilience of replication within systems I through IV, we decided to introduce a larger structural and electronic perturbation into the systems under investigation. This perturbation was the exchange of the 3-substituted furan ring present in systems I through IV for a 2-substituted furan ring that characterises systems V through VIII. Overall, 2-alkyl furans are less reactive than their 3-substituted analogues and the change in substitution pattern introduces significant geometrical change in the structure of the templates.

Systems V and VI: Meaningful analyses of systems V and VI were problematic as a consequence of the low reactivity of diene **3** and dienophiles **5a** and **6a** at 35 °C. Increasing

the reaction temperature to 45 °C did not circumvent the low reactivity, since total conversion to products in uncatalysed bimolecular fusions between **3** and **5b** or **6b** remained in the region of 3 %, whilst in the recognition-mediated reactions between **3** and **5a** or **6a** fashioned products, total conversion was only around 5 %.

System VIII: System VIII is the 2-alkyl furan analogue of system IV. We were interested to discover the effect that the change in furan substitution pattern would have on the reaction pathways adopted by this system. Molecular mechanics calculations (Figure 9) suggested that the structure of *exo*-**14a** is such that reaction through a binary complex is by far

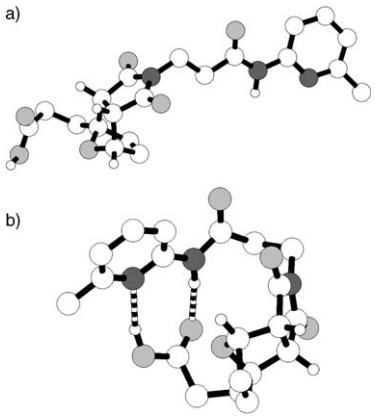

Figure 9. a) Ball-and-stick model of a representative low energy conformation of *endo*-**14a**. b) Ball-and-stick model of a representative low energy conformation of *exo*-**14a**. All structures were calculated using AMBER* force field. Carbon atoms are coloured white, oxygen atoms are coloured light grey, nitrogen atoms are coloured dark grey. Some hydrogen atoms have been omitted for clarity. Hydrogen bonds are represented by dashed lines.

the most likely recognition-mediated process for this system.

Given the low reactivity of the 2-alkyl furan diene, the four kinetic experiments were performed in $CDCl_3$ at 45 °C. Once again, the results are summarised as concentration/time profiles (Figure 10) and in tabular form (Table 6).

It is immediately clear from these results that system VIII does indeed operate predominantly through the binary reactive complex channel. The key evidence is the complete absence of any increase in reaction rate on addition of preformed template. In light of this observation, kinetic simulation and fitting omitted the autocatalytic cycle from the reaction model. Excellent fits of the experimental data to the reaction model were obtained (solid lines in Figure 10). The effective molarity values derived from the simulation and fitting for this system are given in Table 7.

Despite the apparently substantial rate acceleration observed for the formation of *exo*-**14b**, the calculated k_{EM} values are rather low suggesting that the preorganisation of the reactive groups within the binary complex [**4**·**6a**] is poor. Other similar systems described previously by our laboratory have k_{EM} values significantly in excess of 1 M. The unex-

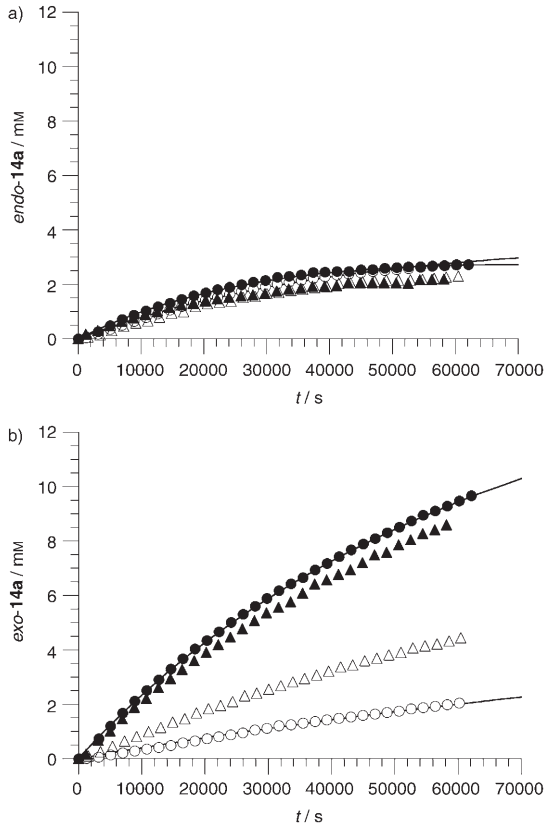

Figure 10. Rate profiles, at 35 °C in $CDCl_3$, for the formation of a) *endo*-**14a** or *endo*-**14b** and b) *exo*-**14a** or *exo*-**14b** from building blocks **4** and **6a** and **4** and **6b**, respectively. Starting concentrations of diene and dienophile were 25 mM. ●: Reaction between **4** and **6a** (Recognition-mediated reaction). ○: Reaction between **4** and **6b** (Bimolecular reaction). △: Reaction between **4** and **6a** in the presence of 4 equiv $PhCO_2H$ (competitive inhibitor). ▲: Reaction between **4** and **6a** in the presence of preformed *endo*-**14a** (10 mol %) or *exo*-**14a** (8 mol %). Solid lines represent the best fit of the experimental data to the appropriate kinetic model using the SimFit[19] package. See Supporting Information for further details of the kinetic models used.

Table 6. Measured initial rates of formation of *endo*-**14** and *exo*-**14** at 45 °C in $CDCl_3$. Relative rates are calculated assuming the reaction between **4** and **6b** has a rate of 1 mM s^{-1}.

Reaction (45 °C/ $CDCl_3$)	r(*endo*-**14**) ($\times 10^{-5}$) [mM s^{-1}]	Relative rate (*endo*-**14**)	r(*exo*-**14**) ($\times 10^{-5}$) [mM s^{-1}]	Relative rate (*exo*-**14**)	Total conversion % (in 16 h)
4 + **6b**	7.56	1.0	3.43	1.0	19
4 + **6a**	9.53	1.2	23.10	6.7	48
4 + **6a** + BA	6.37	0.9	9.15	2.7	16
4 + **6a** + template	8.22	1.1	21.37	6.2	45

Table 7. Calculated kinetic and thermodynamic effective molarity values associated with formation of *endo*-**14a** and *exo*-**14a** through the binary reactive complex pathways at 45 °C in $CDCl_3$.

Reaction pathway (45 °C)	k_{EM}(*endo*-**14a**) [mM]	t_{EM}(*endo*-**14a**) [mM]	k_{EM}(*exo*-**14a**) [mM]	t_{EM}(*exo*-**14a**) [mM]
binary reactive complex	52	639	275	128

pectedly high value of the t_{EM} for *endo*-**14a** (639 mM) indicates that there is a significant level of product ground state stabilisation that is consistent with the result of the molecular mechanics calculations performed on this system. Although an investigation of the effect of temperature on the efficiency of this system would be instructive, investigations at temperatures $T < 45\,^{\circ}C$ were hampered by the low intrinsic reactivities of **4** and **6b** at the lower temperatures.

System VII: Kinetic examination of system VII (Figure 11 and Table 8) reveals striking behavioural similarities with system VIII.

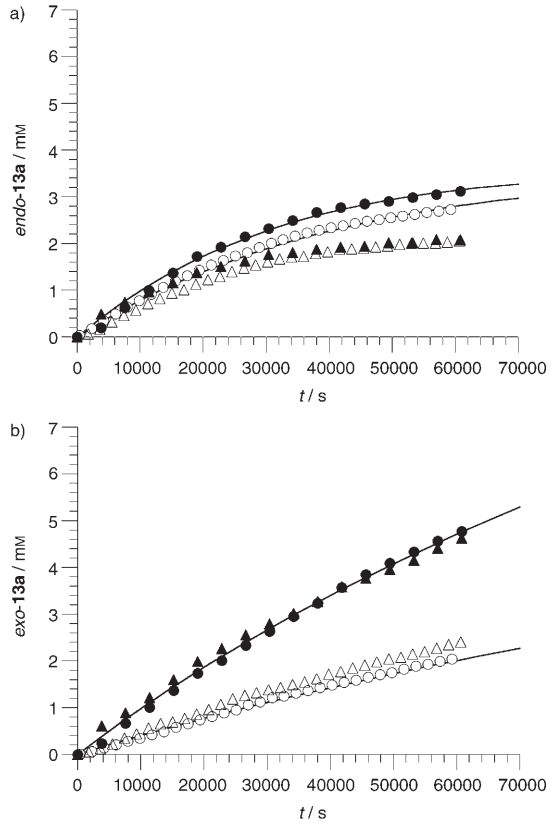

Figure 11. Rate profiles, at 35 °C in $CDCl_3$, for the formation of a) *endo*-**13a** or *endo*-**13b** and b) *exo*-**13a** or *exo*-**13b** from building blocks **4** and **5a** and **4** and **5b**, respectively. Starting concentrations of diene and dienophile were 25 mM. ●: Reaction between **4** and **5a** (recognition-mediated reaction). ○: Reaction between **4** and **5b** (bimolecular reaction). △: Reaction between **4** and **5a** in the presence of 4 equiv $PhCO_2H$ (competitive inhibitor). ▲: Reaction between **4** and **5a** in the presence of preformed *endo*-**13a** (10 mol%) or *exo*-**13a** (8 mol%). Solid lines represent the best fit of the experimental data to the appropriate kinetic model using the SimFit[19] package. See Supporting Information for further details of the kinetic models used.

The formation of the *endo* cycloadduct is essentially unchanged by the introduction of the recognition sites. By contrast, the formation of the *exo* cycloadduct is enhanced by the introduction of recognition. Surprisingly, the magnitude of this rate enhancement is smaller than that observed for system VIII. One could expect that the removal of a rotor

Table 8. Measured initial rates of formation of *endo*-**13** and *exo*-**13** at 45 °C in $CDCl_3$. Relative rates are calculated assuming the reaction between **4** and **5b** has a rate of 1 mM s^{-1}.

Reaction (45 °C/ $CDCl_3$)	r(*endo*-**13**) ($\times 10^{-5}$) [mM s^{-1}]	Relative rate (*endo*-**13**)	r(*exo*-**13**) ($\times 10^{-5}$) [mM s^{-1}]	Relative rate (*exo*-**13**)	Total conversion % (in 16 h)
4 + **5b**	7.84	1.0	3.64	1.0	19
4 + **5a**	9.04	1.1	9.09	2.5	31
4 + **5a** + BA	6.53	0.9	5.11	1.4	18
4 + **5a** + template	8.32	1.0	10.34	2.7	27

in the transformation of system VIII into system VII might make the reaction more favourable entropically[24] by between 13 and 21 eu. This favourable entropy change seems to be offset, in this case, by problems in accessing the correct coconformation in the [**4**·**5a**] complex to permit entry into the *exo* transition state. As expected, calculation of the effective molarity values for this system (Table 9) reveals uniformly low values consistent with the poor performance of this system.

Table 9. Calculated kinetic and thermodynamic effective molarity values associated with formation of *endo*-**14a** and *exo*-**14a** through the binary reactive complex pathways at 45 °C in $CDCl_3$.

Pathway (45 °C)	k_{EM}(*endo*-**13a**) [mM]	t_{EM}(*endo*-**13a**) [mM]	k_{EM}(*exo*-**13a**) [mM]	t_{EM}(*exo*-**13a**) [mM]
binary reactive complex	42	316	140	29

It is worth noting in passing that system III and VII have identical spacers between the recognition sites and the reactive sites. Despite this apparent similarity, the change in substitution pattern in the diene (3-substituted in system III and 2-substituted in system VII) is enough to make their kinetic behaviours entirely different.

Conclusion

By examining the relative rate accelerations achieved (Figure 12) by the eight systems studied here we can extract some important general observations concerning the relationship between structure and function.

It is clear from the data presented in Figure 12 that in three of the four systems based on 3-substituted furans (systems II, III and IV), both diastereoisomers are capable of synthesising themselves through the autocatalytic pathway. In general, the *endo* cycloadducts are slightly more efficient templates than the *exo* cycloadducts since the addition of template (white bars, Figure 12) has a greater effect on the rate enhancement observed. In the case of system I, the system displays no recognition-mediated reactivity at all. A dramatic change in behaviour is brought about by the re-

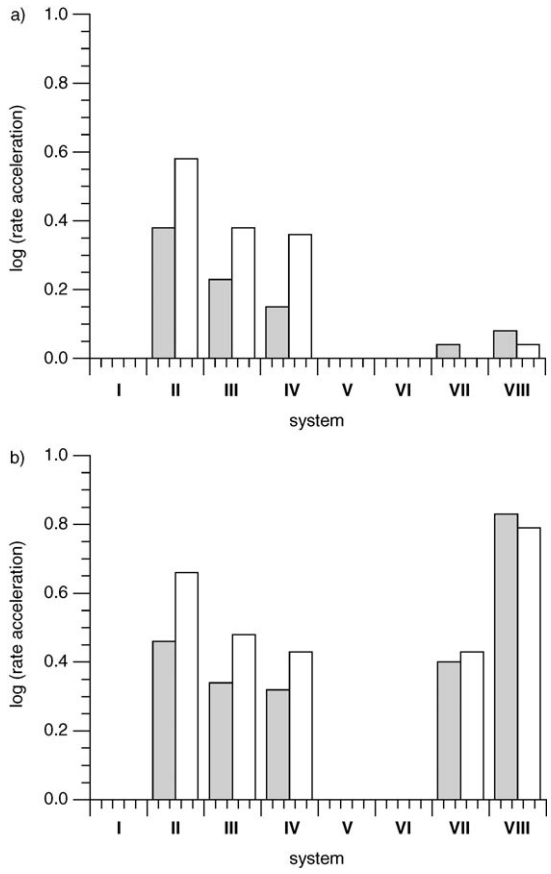

Figure 12. Comparison of the relative rate enhancements observed in a) the *endo* diastereoisomers and b) the *exo* diastereoisomers of the eight systems studied. Rate enhancements are expressed as the $\log_{10}$ of the ratio of the recognition-mediated rate to the bimolecular rate (grey bars) and the $\log_{10}$ of the ratio of the recognition-mediated rate including added template to the bimolecular rate (white bars). No entry for a system signifies that the system does not exhibit measurable recognition-mediated reactivity.

placement of the 3-alkyl furan diene with a 2-alkyl furan diene to create systems V through VIII. In this second group, significant recognition-mediated reactivity is limited to the *exo* cycloadducts of systems VII and VIII and occurs exclusively through the binary reactive complex. The contrast between system II and VI is striking. These two systems are constitutional isomers differing only in the position of substitution on the furan ring. However, whilst in system II both diastereoisomers are rather efficient replicators, system VI shows no recognition-mediated reactivity at all. This observation serves to emphasise the point that the structural window in which replication is observed is rather narrow.

It is instructive to broaden our comparison to include systems described previously[23] by our laboratory. The relationship between the two series of replicators is simple. In the work reported here, the acid recognition site is located on the diene and the amidopyridine recognition site on the dienophile. In the cases reported previously, the acid recognition site is located on the dienophile and the amidopyridine recognition site on the diene. The kinetic behaviours of the systems described here and previously are summarised in Figure 13.

An examination of Figure 13 reveals that the self-replicating behaviour observed in these structurally related systems is clustered in one region only—namely system II, III and IV in the current work. Almost all of the other recognition-mediated reactivity observed occurs through a binary complex reaction channel. An analysis of the number of each type of behaviour observed reveals that, out of 32 potential templates, nine are capable of templating their own formation (of which six are relatively efficient), nine are capable of recognition-mediated reaction through a binary complex channel and 14 are inactive. It would therefore appear that our chances of creating an efficient replicating system successfully even from a rationally designed starting point is only around 1 in 5.

An interesting comparison can also be made between the systems shown in Figure 13b and the work published by von

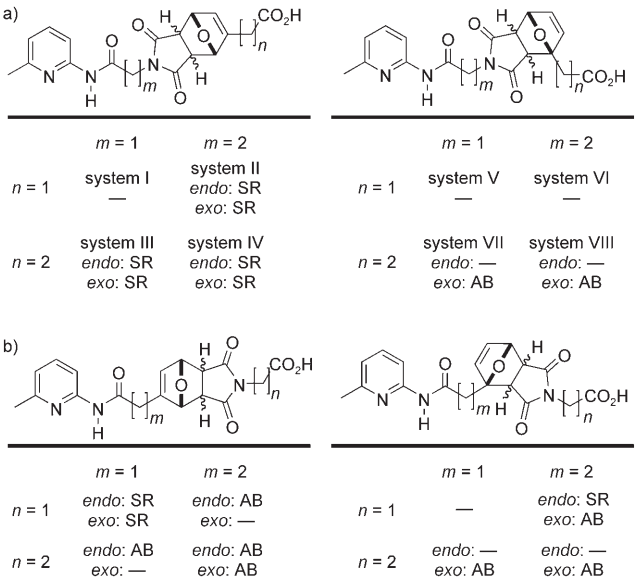

a)	$m = 1$	$m = 2$
$n = 1$	system I —	system II *endo*: SR *exo*: SR
$n = 2$	system III *endo*: SR *exo*: SR	system IV *endo*: SR *exo*: SR

	$m = 1$	$m = 2$
$n = 1$	system V —	system VI —
$n = 2$	system VII *endo*: — *exo*: AB	system VIII *endo*: — *exo*: AB

b)	$m = 1$	$m = 2$
$n = 1$	*endo*: SR *exo*: SR	*endo*: AB *exo*: —
$n = 2$	*endo*: AB *exo*: —	*endo*: AB *exo*: AB

	$m = 1$	$m = 2$
$n = 1$	—	*endo*: SR *exo*: AB
$n = 2$	*endo*: — *exo*: AB	*endo*: — *exo*: AB

Figure 13. a) Kinetic behaviours of the system reported in this work. b) Kinetic behaviours of structurally related systems reported in ref. [23]. The kinetic behaviour of each diastereoisomer is labelled as follows: – = no recognition-mediated reactivity observed. AB = Reaction occurs predominantly through a binary reactive complex. SR = Reaction occurs predominantly through an autocatalytic cycle.

Kiedrowski[8a] on a structurally related system in which the furan component is replaced by a cyclohexadiene. In terms of length of spacer, the most appropriate comparison (Figure 14) is between our system where $m=1$ and $n=1$ (Figure 13b). The cyclohexadiene-based system exhibits nearly exponential replication, whereas the furan-based system shows only weak replication signatures for the *exo* and *endo* diastereoisomers. This striking difference in the observed kinetics of the two systems serves to highlight the fact that the design of predetermined dynamic behaviour is extremely difficult. Presumably, the slight differences in the

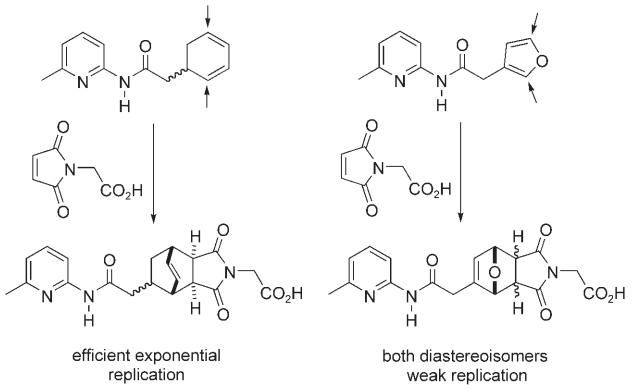

Figure 14. Two structurally related replicating systems have markedly different kinetic behaviour.

location of the diene termini (arrows, Figure 14) and the different inherent reactivity of the furan diene and the cyclohexadiene are responsible for the observed effects. Developing a computational framework that is capable of predicting these subtle differences is a significant challenge.

Moving forward, it is clear that our ultimate goal of developing a robust supramolecular assembly strategy based on replication requires a number of additional developments. Firstly, we must improve the magnitude of the rate accelerations achieved in our systems—the best system described here manages an acceleration of around half an order of magnitude. Secondly, we must use computational methods more in a design role to create systems with a high chance of successfully replicating rather than in a post-rationalisation role. The comparisons drawn in Figures 13 and 14 illustrate that the structural window for replication is narrow and we must exploit modern computational methods to design templates that can be shown computationally to be capable of supporting the transition state leading to themselves. Finally, control and sequencing must be included within our designs in order that replication can be incorporated within more complex kinetic schemes. All of these issues are currently being addressed in our laboratory.

Experimental Section

General procedures: Chemicals and solvents were purchased from Acros Organics, Avocado, Bamford Laboratories, Fisher Scientific, Fluka, Lancaster or Sigma-Aldrich and were used as received unless otherwise stated. Diethyl ether (Et_2O) and tetrahydrofuran (THF) were dried by heating to reflux in the presence of sodium/benzophenone under an N_2 atmosphere and were collected by distillation. Acetonitrile (CH_3CN), *N,N′*-dimethylformamide (DMF) and CH_2Cl_2 were dried by heating under reflux over calcium hydride and distilled under N_2.

Thin-layer chromatography (TLC) was performed on aluminium plates coated with Merck Kieselgel 60 F_{254}. Developed plates were air-dried and scrutinised under a UV lamp (366 nm), and where necessary, stained with iodine, phosphomolybdic acid (PMA) or ninhydrin or potassium permanganate to aid visualisation. Column chromatography was performed using Kieselgel 60 (0.040–0.063 mm mesh, Merck 9385) or MP Silica (silica gel, 0.032–0.063 mesh).

Melting points were determined using an Electrothermal 9200 melting point apparatus and are uncorrected. Microanalyses (CHN) were carried out at the University of St Andrews. Infra-red Spectra (IR) were recorded as KBr discs or thin films (PTFE plates) using a Perkin–Elmer Paragon 1000 spectrometer.

^{1}H Nuclear magnetic resonance (NMR) spectra were recorded on a Bruker Avance 300 (300.1 MHz), a Varian Gemini 2000 (300.0 MHz), a Bruker Avance 500 (500.0 MHz) or a Varian UNITYplus 500 (500.1 MHz) spectrometer using the deuterated solvent as the lock and the residual solvent as the internal reference in all cases. ^{13}C NMR spectra using the PENDANT sequence were recorded on a Bruker Avance 300 (75.5 MHz) spectrometer. All other ^{13}C spectra were recorded on a Varian Gemini 2000 (75.5 MHz) spectrometer using composite pulse ^{1}H decoupling. ^{19}F NMR spectra were recorded on a Bruker Avance 300 (282.3 MHz) spectrometer using the deuterated solvent as the lock and the residual solvent as the internal reference. All spectra were recorded at 298 K unless otherwise stated. All coupling constants are quoted to the nearest 0.1 Hz. In the assignment of ^{1}H NMR spectra the symbols br, s, d, t, q, and m denote broad, singlet, doublet, triplet, quartet and multiplet, respectively.

Electron impact mass spectrometry (EIMS) and high-resolution mass spectrometry (HRMS) were carried out on a VG AUTOSPEC mass spectrometer or on a Micromass GCT orthogonal acceleration time of flight mass spectrometer. Chemical Ionisation Mass Spectrometry (CIMS) was carried out on a VG AUTOSPEC instrument or on a Micromass GCT orthogonal acceleration time of flight mass spectrometer. Electrospray mass spectrometry (ESMS) and high-resolution mass spectrometry (HRMS) was carried out on a Micromass LCT orthogonal time of flight mass spectrometer.

General procedure for kinetic experiments: Stock solutions of precursory subunits and/or additives (templates, inhibitors) were prepared by dissolving the appropriate amount of reagent in $CDCl_3$ using Volac 5 mL ± 0.025 mL or 2 mL ± 0.015 mL volumetric flasks. Masses of reagents were measured using a Sartorius BP 211D balance (± 0.01 mg). Stock solutions were pre-equilibrated to the appropriate temperature in a water bath for a minimum 30 minutes. Miscellaneous reaction mixtures were prepared by sequential injection of appropriate volumes of reagent solutions (precursory subunits, templates, inhibitors) into a Wilmad 507 or 528PP NMR tube, which was subsequently fitted with a polyethylene pressure cap to minimise solvent evaporation. Volumes of reagent solutions were measured accurately via utilisation of a 1.0 or 0.5 mL Hamilton gas tight syringe. Reaction mixtures were monitored systematically (spectra recorded every 790, 1890 or 1900 s) by 500 MHz ^{1}H NMR over 16 h. The extent of reaction for kinetic experiments was determined using the deconvolution tool available in 1D WINNMR (Version 6.2.0.0, Bruker Daltonik GmbH, Germany, 2000). Kinetic simulation and fitting of the resultant data to the appropriate kinetic models was achieved using the fitting mode of SimFit.[19]

Computational methods: All molecular mechanics calculations were performed on a Linux workstation the AMBER* force field together with the GB/SA solvation model for chloroform as implemented in Macromodel (Version 7.1, Schrodinger Inc., 2000). Ab initio electronic structure calculations were carried out using GAMESS[25] running on a Linux cluster. The version dated 22 November 2004 was used in all calculations. The transition state for the reaction between furan and maleimide was located by generation of an initial guess using the linear synchronous transit (LST) method and then refinement at the HF/6-31G(d) level of theory within GAMESS. This model transition state was then used to construct an initial guess for the transition state leading to the appropriate cycloadduct. This guess was refined at the B3LYP/6-31G(d) level of theory to a transition state structure possessing single imaginary vibration that corresponded to the reaction coordinate.

Synthetic procedures

Preparative methods and characterisation data for compounds **1**, **2**, **3**, **4**, **5a**, **5b**, **6a**, **6b** are provided in the Supporting Information.

{4-[(6-Methyl-pyridin-2-ylcarbamoyl)-methyl]-3,5-dioxo-10-oxa-4-aza-tricyclo[5.2.1.0^{2,6}]dec-8-en-8-yl} acetic acid (*endo*-7a and *exo*-7a): A 1:1 mixture of **1** (0.5 mL of a 50 mM solution in $CDCl_3$) and **5a** (0.5 mL of a

50 mM solution in $CDCl_3$) in an NMR tube was heated at 50 °C for 2 d. Adducts *endo*-**7a** and *exo*-**7a** (5.4 mg, 58 %, inseparable mixture of diastereoisomers, *endo*-**7a**/*exo*-**7a** 1:1) precipitated from the reaction mixture as a colourless crystalline solid and were subsequently filtered off and washed with copious amounts of $CHCl_3$. M.p. 205.8–208.1 °C; ^{1}H NMR (500 MHz, [D$_6$]DMSO, 25 °C, TMS): δ = 10.65 (brs, 1H$_{exo}$), 10.61 (brs, 1H$_{endo}$), 7.75 (d, 1H$_{endo}$, 1H$_{exo}$, J = 7.0 Hz), 7.63 (t, 1H$_{endo}$, 1H$_{exo}$, J = 7.7 Hz), 6.96 (d, 1H$_{endo}$, 1H$_{exo}$, J = 7.6 Hz), 6.30 (d, 1H$_{exo}$, J = 1.5 Hz), 6.11 (br, 1H$_{endo}$), 5.27 (d, 1H$_{endo}$, J = 4.6 Hz), 5.23 (d, 1H$_{endo}$, J = 4.7 Hz), 5.10 (br, 1H$_{exo}$), 5.06 (s, 1H$_{exo}$), 4.23 (s, 2H$_{exo}$), 4.09 (s, 2H$_{endo}$), 3.67 (m, 2H$_{endo}$), 3.33 (s, 2H$_{exo}$), 3.26 (d, 1H$_{exo}$, J = 6.6 Hz), 3.18 (d, 1H$_{endo}$, J = 17.3 Hz), 3.09 (d, 1H$_{exo}$, J = 6.6 Hz), 2.94–2.90 (dd, 1H$_{endo}$, J = 1.8, 17.9 Hz), 2.40 (s, 3H$_{exo}$), 2.39 (s, 3H$_{endo}$); ^{13}C NMR (125 MHz, [D$_6$]DMSO, 25 °C, TMS, *endo*-**7a** in parentheses): δ = 175.9, 175.7, (174.3), (174.0), 171.1, (170.8), 164.6, 156.5, 150.7, 144.1, (142.7), (142.4), (140.2), 138.4, (134.8), 132.3, 129.5, 118.7, (111.7), (110.3), 110.2, 82.3, 80.9, (80.3), (79.3), 48.4, (47.0), 46.8, (45.9), 41.0, (40.7), (33.7), 32.8, (30.2), (23.4); IR (KBr): $\tilde{\nu}$ = 3464, 3079, 2995, 1712, 1616, 1582, 1457, 1409, 1327, 1265, 1226, 1169 cm^{-1}; MS (ES−): *m*/*z* (%): 370 (5) [*M*−H]$^+$; HRMS (ES−): *m*/*z*: calcd for $C_{18}H_{16}N_3O_6$: 370.1039, found 370.1033 [*M*−H]$^+$.

{4-[2-(6-Methylpyridin-2-ylcarbamoyl)-ethyl]-3,5-dioxo-10-oxa-4-aza-tricyclo[5.2.1.0^{2,6}]dec-8-en-8-yl} acetic acid (*endo*-8a and *exo*-8a): A 1:1 mixture of **1** (0.5 mL of a 50 mM solution in $CDCl_3$) and **6a** (0.5 mL of a 50 mM solution in $CDCl_3$) in an NMR tube was heated at 50 °C for 2 d. Adducts *endo*-**8a** and *exo*-**8a** (6.1 mg, 63 %, inseparable mixture of diastereoisomers, *endo*-**8a**/*exo*-**8a** 1:1) precipitated from the reaction mixture as a colourless crystalline solid and were subsequently filtered off and washed with copious amounts of $CHCl_3$. M.p. 172.0–173.1 °C; ^{1}H NMR (500 MHz, [D$_6$]DMSO, 25 °C, TMS): δ = 12.43 (br, 1H$_{endo}$, 1H$_{exo}$), 10.39 (br, 1H$_{endo}$, 1H$_{exo}$), 7.84 (d, 1H$_{endo}$, 1H$_{exo}$, J = 8.4 Hz), 7.65 (t, 1H$_{endo}$, J = 8.0 Hz), 7.64 (t, 1H$_{exo}$, J = 8.1 Hz), 6.96 (d, 1H$_{endo}$, 1H$_{exo}$, J = 7.3 Hz), 6.30 (d, 1H$_{exo}$, J = 1.5 Hz), 6.10 (br, 1H$_{endo}$), 5.27 (d, 1H$_{endo}$, J = 5.1 Hz), 5.22 (d, 1H$_{endo}$, J = 5.3 Hz), 5.07 (s, 1H$_{exo}$), 5.03 (br, 1H$_{exo}$), 3.6 (t, 2H$_{exo}$, J = 7.6 Hz), 3.59 (q, 2H$_{endo}$, J = 5.0 Hz), 3.50 (dd, 2H$_{endo}$, J = 7.9, 15.2 Hz), 3.34 (s, 2H$_{exo}$), 3.18 (d, 1H$_{endo}$, J = 2.6 Hz), 3.17 (d, 1H$_{exo}$, J = 6.3 Hz), 2.99 (d, 1H$_{exo}$, J = 6.3 Hz), 2.93–2.89 (dd, 1H$_{endo}$, J = 1.9, 17.5 Hz), 2.61 (t, 2H$_{exo}$, J = 7.6 Hz), 2.53–2.50 (m, 2H$_{endo}$), 2.41 (s, 3H$_{endo}$, 3H$_{exo}$); ^{13}C NMR (125 MHz, [D$_6$]DMSO, 25 °C, TMS, *endo*-**8a** in parentheses): δ = 176.2, (176.0), (174.6), 174.3, (171.1), 170.6, (169.3), (169.0), 169.0, (161.8), 156.2, 151.1, 144.0, 142.7, (140.2), (138.1), (134.4), 132.2, 129.1, 118.4, (111.7), 110.4, (110.3), 82.3, 80.9, (80.3), (79.3), (54.4), (48.2), 46.6, 45.5, (34.2), 32.8, 32.4, (26.7), 23.4; IR (KBr): $\tilde{\nu}$ = 3449, 3276, 3074, 2353, 1700, 1616, 1577, 1452, 1399, 1323, 1260, 1193, 1159 cm^{-1}; MS (ES−): *m*/*z* (%): 384 (100) [*M*−H]$^+$; HRMS (ES−): *m*/*z*: calcd for $C_{19}H_{18}N_3O_6$: 384.1196, found 384.1202 [*M*−H]$^+$.

***exo*-3-{4-[(6-Methyl-pyridin-2-ylcarbamoyl)-methyl]-3,5-dioxo-10-oxa-4-aza-tricyclo[5.2.1.0^{2,6}]dec-8-en-8-yl} propionic acid (*exo*-9a)**: A 1:1 mixture of **2** (0.5 mL of a 50 mM solution in $CDCl_3$) and **5a** (0.5 mL of a 50 mM solution in $CDCl_3$) in an NMR tube was heated at 35 °C for 3 d. *exo*-**9a** (3.9 mg, 40 %) precipitated from the reaction mixture as a colourless crystalline solid and was subsequently filtered off and washed with copious amounts of $CHCl_3$. M.p. 179.5–180.4 °C; ^{1}H NMR (500 MHz, [D$_6$]DMSO, 25 °C, TMS): δ = 10.64 (br s, 1H), 7.75 (d, 1H, J = 7.5 Hz), 7.62 (t, 1H, J = 7.7 Hz), 6.95 (d, 1H, J = 7.5 Hz), 6.09 (brs, 1H), 5.07 (br, 1H), 5.00 (br s, 1H), 4.23 (brs, 2H), 3.10 (d, 1H, J = 6.4 Hz), 3.02 (d, 1H, J = 6.5 Hz), 2.47–2.41 (m, 4H), 2.40 (s, 3H); ^{13}C NMR (125 MHz, [D$_6$]DMSO, 25 °C, TMS): δ = 175.8, 175.6, 173.4, 164.5, 156.4, 150.7, 150.1, 138.4, 128.7, 118.7, 110.2, 82.2, 81.0, 48.8, 46.7, 41.0, 31.4, 23.4, 21.9; IR (KBr): $\tilde{\nu}$ = 3440, 3238, 3074, 2372, 1700, 1585, 1460, 1421, 1325, 1267, 1209, 1161 cm^{-1}; MS (ES−): *m*/*z* (%): 384 (100) [*M*−H]$^+$; HRMS (ES−): *m*/*z*: calcd for $C_{19}H_{18}N_3O_6$: 384.1196, found 384.1193 [*M*−H]$^+$.

***exo*-3-{4-[2-(6-methyl-pyridin-2-ylcarbamoyl)-ethyl]-3,5-dioxo-10-oxa-4-azatricyclo[5.2.1.0^{2,6}]dec-8-en-8-yl} propionic acid (*exo*-10a)**: A 1:1 mixture of **2** (0.5 mL of a 50 mM solution in $CDCl_3$) and **6a** (0.5 mL of a 50 mM solution in $CDCl_3$) in an NMR tube was heated at 45 °C for 3 d. *exo*-**10a** (4.0 mg, 40 %) precipitated from the reaction mixture as a colourless crystalline solid and was subsequently filtered off and washed with copious amounts of $CHCl_3$. M.p. 211.8–212.9 °C; ^{1}H NMR (500 MHz, [D$_6$]DMSO, 25 °C, TMS): δ = 10.39 (brs, 1H), 7.84 (d, 1H, J = 8.0 Hz), 7.64 (t, 1H, J = 7.8 Hz), 6.95 (d, 1H, J = 7.4 Hz), 6.10 (brs, 1H), 5.06 (br, 1H), 4.98 (s, 1H), 3.65 (t, 2H, J = 7.4 Hz), 3.01 (d, 1H, J = 6.6 Hz), 2.94 (d, 1H, J = 6.6 Hz), 2.62 (t, 2H, J = 7.4 Hz), 2.47–2.43 (m, 4H), 2.40 (s, 3H); ^{13}C NMR (125 MHz, [D$_6$]DMSO, 25 °C, TMS): δ = 176.1, 176.0, 173.5, 169.1, 156.3, 151.1, 150.1, 138.2, 128.7, 118.4, 110.5, 82.3, 81.0, 48.7, 46.6, 34.2, 33.8, 31.4, 23.4, 22.0; IR (KBr): $\tilde{\nu}$ = 3464, 3079, 2995, 1712, 1616, 1582, 1457, 1409, 1327, 1265, 1226, 1169 cm^{-1}; MS (ES−): *m*/*z* (%): 398 (70) [*M*−H]$^+$; HRMS (ES−): *m*/*z*: calcd for $C_{20}H_{20}N_3O_6$: 398.1352, found 398.1356 [*M*−H]$^+$.

***exo*-{4-[(6-Methyl-pyridin-2-ylcarbamoyl)-methyl]-3,5-dioxo-10-oxa-4-aza-tricyclo[5.2.1.0^{2,6}]dec-8-en-1-yl} acetic acid (*exo*-11a)**: A 1:1 mixture of **3** (0.5 mL of a 50 mM solution in $CDCl_3$) and **5a** (0.5 mL of a 50 mM solution in $CDCl_3$) in an NMR tube was heated at 45 °C for 4 d. *exo*-**11a** (3.1 mg, 33 %) precipitated from the reaction mixture as a colourless crystalline solid and was subsequently filtered off and washed with copious amounts of $CHCl_3$. M.p. 151.4–152.5 °C; ^{1}H NMR (500 MHz, [D$_6$]DMSO, 25 °C, TMS): δ = 10.59 (brs, 1H), 7.74 (d, 1H, J = 7.7 Hz), 7.63 (t, 1H, J = 7.7 Hz), 6.96 (d, 1H, J = 7.3 Hz), 6.36 (brs, 2H), 5.26 (d, 1H, J = 5.5 Hz), 4.08 (s, 2H), 3.77–3.74 (dd, 1H, J = 5.5, 7.5 Hz), 3.61 (d, 1H, J = 7.7 Hz), 3.05 (d, H, J = 15.0 Hz), 2.97 (d, 1H, J = 15.0 Hz), 2.39 (s, 3H); ^{13}C NMR (125 MHz, [D$_6$]DMSO, 25 °C, TMS): δ = 174.1, 174.0, 170.4, 164.4, 156.4, 150.6, 138.4, 134.8, 133.6, 118.7, 110.2, 87.2, 78.4, 48.7, 47.8, 40.7, 33.5, 23.4; IR (KBr): $\tilde{\nu}$ = 3444, 2358, 1770, 1698, 1457, 1399, 1323, 1159 cm^{-1}; MS (ES−): *m*/*z* (%): 370 (100) [*M*−H]$^+$; HRMS (ES−): *m*/*z*: calcd for $C_{18}H_{16}N_3O_6$: 370.1039, found 370.1043 [*M*−H]$^+$.

{4-[2-(6-Methyl-pyridin-2-ylcarbamoyl)-ethyl]-3,5-dioxo-10-oxa-4-azatri-cyclo[5.2.1.0^{2,6}]dec-8-en-1-yl} acetic acid (*endo*-12a and *exo*-12a): A 1:1 mixture of **3** (0.5 mL of a 50 mM solution in $CDCl_3$) and **6a** (0.5 mL of a 50 mM solution in $CDCl_3$) in an NMR tube was heated at 45 °C for 4 d. Adducts *endo*-**12a** and *exo*-**12a** (2.4 mg, 25 %, inseparable mixture of diastereoisomers: *endo*-**12a**/*exo*-**12a** 1:3) precipitated from the reaction mixture as a colourless crystalline solid and were subsequently filtered off and washed with copious amounts of $CHCl_3$. M.p. 180.4–180.9 °C; ^{1}H NMR (500 MHz, [D$_6$]DMSO, 25 °C, TMS): δ = 10.39 (br, 1H$_{exo}$), 10.34 (br, 1H$_{endo}$), 7.84 (d, 1H$_{exo}$, J = 7.6 Hz), 7.84 (d, 1H$_{endo}$, J = 7.6 Hz), 7.65 (t, 1H$_{endo}$, J = 7.6 Hz), 7.63 (t, 1H$_{exo}$, J = 7.7 Hz), 6.95 (d, 1H$_{exo}$, J = 7.5 Hz), 6.95 (d, 1H$_{endo}$, J = 7.5 Hz), 6.56 (d, 1H$_{exo}$, J = 1.3 Hz), 6.55 (d, 1H$_{exo}$, J = 5.7 Hz), 6.36 (d, 1H$_{endo}$, J = 5.7 Hz), 6.31 (d, 1H$_{endo}$, J = 5.6 Hz), 5.24 (dd, 1H$_{endo}$, J = 1.2, 5.5 Hz), 5.07 (d, 1H$_{exo}$, J = 1.4 Hz), 3.65 (dt, 2H$_{exo}$, J = 3.4, 9.0 Hz), 3.53–3.48 (m, 4H$_{endo}$), 3.08 (d, 1H$_{exo}$, J = 6.5 Hz), 3.08–3.05 (d, 1H$_{endo}$, J = 15.5 Hz), 3.02 (d, 1H$_{exo}$, J = 6.5 Hz), 2.98–2.95 (d, 1H$_{endo}$, J = 15.2 Hz), 2.95 (d, 1H$_{exo}$, J = 16.9 Hz), 2.91 (d, 1H$_{exo}$, J = 16.9 Hz), 2.64–2.60 (dt, 2H$_{exo}$, J = 2.6, 7.2 Hz), 2.54 (t, 2H$_{endo}$, J = 7.3 Hz), 2.40 (brs, 3H$_{exo}$, 3H$_{endo}$); ^{13}C NMR (125 MHz, [D$_6$]DMSO, 25 °C, TMS, *endo*-**12a** in parentheses): δ = 175.8, 174.6, (174.6), (174.4), 170.6, (170.0), (169.1), 169.1, (156.3), 156.3, 151.2, 139.0, (138.3), 138.2, (136.4), 136.3, (134.5), (133.5), 118.4, 110.5, (110.3), (87.6), (87.0), 79.7, (78.5), 49.8, 48.4, 47.4, (39.8), (37.0), 34.4, 34.2, (33.9), 33.8, (33.5), 23.4; IR (KBr): $\tilde{\nu}$ = 3459, 3276, 3122, 3084, 2949, 2372, 1772, 1700, 1618, 1575, 1455, 1397, 1320, 1157 cm^{-1}; MS (ES−): *m*/*z* (%): 384 (100) [*M*−H]$^+$; HRMS (ES−): *m*/*z*: calcd for $C_{19}H_{18}N_3O_6$: 384.1196, found 384.1186 [*M*−H]$^+$.

***exo*-{4-[(6-methylpyridin-2-ylcarbamoyl)-methyl]-3,5-dioxo-10-oxa-4-aza-tricyclo[5.2.1.0^{2,6}]dec-8-en-1-yl} propionic acid (*exo*-13a)**: A 1:1 mixture of **4** (0.5 mL of a 50 mM solution in $CDCl_3$) and **5a** (0.5 mL of a 50 mM solution in $CDCl_3$) in an NMR tube was heated at 50 °C for 2 d. *exo*-**13a** (4.4 mg, 46 %) precipitated from the reaction mixture as a colourless crystalline solid and was subsequently filtered off and washed with copious amounts of $CHCl_3$. M.p. 191.0–191.5 °C; ^{1}H NMR (500 MHz, [D$_6$]DMSO, 25 °C, TMS): δ = 12.10 (brs, 1H), 10.68 (brs, 1H), 7.78 (d, 1H, J = 7.0 Hz), 7.66 (t, 1H, J = 7.7 Hz), 6.99 (d, 1H, J = 7.5 Hz), 6.59 (d, 1H, J = 5.5 Hz), 6.51 (d, 1H, J = 5.6 Hz), 5.12 (d, 1H, J = 1.3 Hz), 4.27 (d, 2H, J = 4.0 Hz), 3.20 (d, 1H, J = 6.6 Hz), 3.01 (d, 1H, J = 6.5 Hz), 2.57–2.48 (m, 1H), 2.44–2.37 (m, 1H), 2.43 (s, 3H), 2.13–2.07 (m, 1H); ^{13}C NMR (125 MHz, [D$_6$]DMSO, 25 °C, TMS): δ = 175.6, 174.3, 173.7, 164.5, 156.5, 150.7, 138.4, 138.2, 137.2, 118.7, 110.2, 90.4, 79.8, 50.2, 48.7, 41.0, 29.5, 24.6, 23.4; IR (KBr): $\tilde{\nu}$ = 3448, 3209, 3064, 2362, 1777, 1710,

1585, 1455, 1416, 1335, 1262, 1209, 1171 cm^{-1}; MS (ES−): *m/z* (%): 384 (100) $[M-H]^+$; HRMS (ES−): *m/z*: calcd for $C_{19}H_{18}N_3O_6$: 384.1196, found 384.1188 $[M-H]^+$.

3-{4-[2-(6-Methylpyridin-2-ylcarbamoyl)-ethyl]-3,5-dioxo-10-oxa-4-azatricyclo[5.2.1.0^{2,6}]dec-8-en-1-yl} propionic acid (*endo*-14a and *exo*-14a): A 1:1 mixture of **4** (0.5 mL of a 50 mM solution in $CDCl_3$) and **6a** (0.5 mL of a 50 mM solution in $CDCl_3$) in an NMR tube was heated at 50 °C for 2 d. Adducts *endo*-**14a** and *exo*-**14a** (3.5 mg, 35%, mixture of diastereoisomers: *endo*-**14a**/*exo*-**14a**, 1:3) precipitated from the reaction mixture as a colourless crystalline solid and were subsequently filtered off and washed with copious amounts of $CHCl_3$. M.p. 149.4–150.9 °C; ^{1}H NMR (500 MHz, [D$_6$]DMSO, 25 °C, TMS): $\delta = 10.37$ (br s, 1H$_{exo}$), 10.33 (br, 1H$_{endo}$), 7.81 (d, 1H$_{exo}$, $J = 8.2$ Hz), 7.81 (d, 1H$_{endo}$, $J = 8.2$ Hz), 7.61 (t, 1H$_{endo}$, $J = 7.7$ Hz), 7.59 (t, 1H$_{exo}$, $J = 7.7$ Hz), 6.91 (d, 1H$_{endo}$, $J = 7.3$ Hz), 6.90 (d, 1H$_{exo}$, $J = 7.3$ Hz), 6.52 (dd, 1H$_{exo}$, $J = 1.3$, 5.7 Hz), 6.43 (d, 1H$_{exo}$, $J = 5.7$ Hz), 6.32 (d, 1H$_{endo}$, $J = 5.7$ Hz), 6.27 (d, 1H$_{endo}$, $J = 5.6$ Hz), 5.19 (dd, 1H$_{endo}$, $J = 1.3$, 5.5 Hz), 5.03 (d, 1H$_{exo}$, $J = 1.5$ Hz), 3.65–3.58 (m, 2H$_{exo}$), 3.47 (t, 2H$_{endo}$, $J = 7.4$ Hz), 3.24 (d, 1H$_{endo}$, $J = 7.4$ Hz), 3.02 (d, 1H$_{exo}$, $J = 6.5$ Hz), 2.83 (d, 1H$_{exo}$, $J = 6.5$ Hz), 2.83–2.80 (dd, 1H$_{endo}$, $J = 8.0$, 9.1 Hz), 2.64–2.60 (dt, 2H$_{exo}$, $J = 2.2$, 7.9 Hz), 2.50 (t, 2H$_{endo}$, $J = 7.3$ Hz), 2.45–2.02 (m, 7H$_{exo}$, 7H$_{endo}$); ^{13}C NMR (125 MHz, [D$_6$]DMSO, 25 °C, TMS, *endo*-**12a** in parentheses): $\delta = 176.1$, (174.9), 174.7, 174.0, (173.9), (173.5), (171.8), (169.3), 169.2, (156.4), 156.4, 151.3, (138.5), 138.4, 138.3, 137.3, (136.1), (135.2), 118.6, 110.6, (110.4), (90.5), (90.4), 80.0, (78.3), 50.2, (49.2), 48.7, (47.9), 34.7, (34.3), (34.0), 33.9, (33.6), 32.0, 29.7, (29.2), (27.2), 24.7, 23.6; IR (KBr): $\tilde{\nu} = 3444$, 3213, 3079, 2934, 2357, 1770, 1702, 1611, 1577, 1452, 1395, 1327, 1159 cm^{-1}; MS (ES−): *m/z* (%): 398 (100) $[M-H]^+$; HRMS (ES−): *m/z*: calcd for $C_{20}H_{20}N_3O_6$: 398.1352, found 398.1351 $[M-H]^+$.

***endo*-3-{4-[(Methylphenylcarbamoyl)-ethyl]-3,5-dioxo-10-oxa-4-azatricyclo[5.2.1.0^{2,6}]dec-8-en-8-yl} propionic acid (*endo*-10b)**: A 1:1 mixture of **2** (0.5 mL of a 50 mM solution in $CDCl_3$) and **6b** (0.5 mL of a 50 mM solution in $CDCl_3$) in an NMR tube was heated at 50 °C for 5 d. Subsequently, the solvent was removed under reduced pressure and the crude product was purified via column chromatography (silica gel, hexane/EtOAc 2:1), affording *endo*-**10b** (3.8 mg, 38%) as a colourless oil. ^{1}H NMR (500 MHz, $CDCl_3$, 25 °C, TMS): $\delta = 7.45$–7.16 (m, 5H), 5.82 (br, 1H), 5.18 (d, 1H, $J = 4.2$ Hz), 5.03 (d, 1H, $J = 4.2$ Hz), 3.56 (t, 2H, $J = 7.6$ Hz), 3.47 (m, 2H), 3.22 (s, 3H), 2.44–2.13 (m, 6H); ^{13}C NMR (125 MHz, $CDCl_3$, 25 °C, TMS): $\delta = 176.1$, 174.6, 174.1, 169.8, 148.8, 143.2, 129.8, 128.1, 127.1, 126.4, 81.3, 80.1, 47.1, 46.0, 37.2, 34.7, 31.5, 31.2, 23.2; IR (KBr): $\tilde{\nu} = 3444$, 2969, 2365, 1962, 1646, 1582, 1453, 1400, 1327, 1265, 1246, 1120 cm^{-1}; MS (ES−): *m/z* (%): 397 (100) $[M-H]^+$, 353 (25); HRMS (ES−): *m/z*: calcd for $C_{21}H_{21}N_2O_6$: 397.1400, found 397.1403 $[M-H]^+$.

3-{4-[2-(Methylphenylcarbamoyl)-ethyl]-3,5-dioxo-10-oxa-4-azatricyclo[5.2.1.0^{2,6}]dec-8-en-1-yl} propionic acid (*endo*-14b and *exo*-14b): A 1:1 mixture of **4** (0.5 mL of a 50 mM solution in $CDCl_3$) and **6b** (0.5 mL of a 50 mM solution in $CDCl_3$) in an NMR tube was heated at 50 °C for 5 d. Subsequently, the solvent was removed under reduced pressure and the crude product was purified via column chromatography (silica gel, hexane/EtOAc 2:1), affording adducts *endo*-**14b** and *exo*-**14b** (2.9 mg, 29%, inseparable mixture of diastereoisomers: *endo*-**14a**/*exo*-**14a** 1:2) as a colourless oil. ^{1}H NMR (500 MHz, $CDCl_3$, 25 °C, TMS): $\delta = 7.45$–7.16 (m, 5H$_{exo}$, 5H$_{endo}$), 6.49 (d, 1H$_{exo}$, $J = 5.8$ Hz), 6.32 (d, 1H$_{exo}$, $J = 5.8$ Hz), 6.21 (d, 1H$_{endo}$, $J = 5.8$ Hz), 6.07 (d, 1H$_{endo}$, $J = 5.8$ Hz), 5.19–5.14 (m, 1H$_{exo}$, 1H$_{endo}$), 3.79–3.63 (m, 2H$_{exo}$), 3.59–3.50 (m, 3H$_{endo}$), 3.22 (s, 3H$_{exo}$, 3H$_{endo}$), 3.11 (d, 1H$_{endo}$, $J = 7.8$ Hz), 2.90 (d, 1H$_{exo}$, $J = 6.5$ Hz), 2.65–2.29 (m, 6H$_{exo}$, 4H$_{endo}$), 2.21 (t, 2H$_{endo}$, $J = 7.6$ Hz); ^{13}C NMR (125 MHz, $CDCl_3$,, 25 °C, TMS *endo*-**14b** in parentheses): $\delta = 177.0$, (176.9), 175.6, (174.5), (174.4), 174.3, 169.8, (169.6), 143.5, (143.4), 138.2, 137.6, (135.7), (135.4), 129.9, (128.0), 127.2, (90.8), 90.6, 80.4, (78.9), 50.4, (49.5), 48.9, (48.3), 37.3, (37.1), 35.3, (34.8), (31.6), 31.5, 29.6, (29.1), (27.0), 24.4; IR (KBr): $\tilde{\nu} = 3399$, 3086, 2934, 2357, 1624, 1570, 1459, 1399, 1327, 1119 cm^{-1}; MS (ES−) *m/z* (%): 397 (100) $[M-H]^+$; HRMS (ES−): *m/z*: calcd for $C_{21}H_{21}N_2O_6$: 397.1400, found 397.1393 $[M-H]^+$.

Acknowledgements

BBSRC (Grant 6/11855), EPSRC (DTA award to E.K.) and the University of St Andrews supported this work financially. We are grateful to Caroline Horsburgh (Mass spectrometry) and Melanja Smith (NMR) for technical assistance. We thank Prof G. von Kiedrowski for providing us with a copy of his SimFit program.

[1] For examples of complex replicable entities see: a) L.-H. Eckardt, K. Naumann, W. M. Pankau, M. Rein, M. Schweitzer, N. Windhab, G. von Kiedrowski, *Nature* **2002**, *420*, 286; b) J. W. Szostak, D. P. Bartel, P. L. Luisi, *Nature* **2001**, *409*, 387–390; c) N. C. Seeman, P. S. Lukeman, *Rep. Prog. Phys.* **2005**, *68*, 237–270; d) R. Wick, P. Walde, P. L. Luisi, *J. Am. Chem. Soc.* **1995**, *117*, 1435–1436; e) A. Veronese, P. L. Luisi, *J. Am. Chem. Soc.* **1998**, *120*, 2662–2663.

[2] a) A. Mulder, J. Huskens and D. N. Reinhoudt, *Org. Biomol. Chem.* **2004**, *2*, 3409–3424; b) G. M. Whitesides, M. Boncheva, *Proc. Natl. Acad. Sci. USA* **2002**, *99*, 4769–4774; c) G. M. Whitesides, B. Grzybowski, *Science* **2002**, *295*, 2418–2421; d) H. Cölfen, S. Mann, *Angew. Chem.* **2003**, *115*, 2452–2468; *Angew. Chem. Int. Ed.* **2003**, *42*, 2350–2365; e) I. W. Hamley, *Angew. Chem.* **2003**, *115*, 1730–1752; *Angew. Chem. Int. Ed.* **2003**, *42*, 1692–1712; f) G. W. Gokel, W. M. Leevy, M. E. Weber, *Chem. Rev.* **2004**, *104*, 2723–2750, and references therein; g) J. W. Lee, S. Samal, N. Selvapalam, H.-J. Kim, K. Kim, *Acc. Chem. Res.* **2003**, *36*, 621–630, and references therein; h) F. W. B. van Leeuwen, H. Beijleveld, H. Kooijman, A. L. Spek, W. Veboom, D. N. Reinhoudt, *J. Org. Chem.* **2004**, *69*, 3928–3936, and references therein; i) R. Martínez-Mánez, F. Sancenón, *Chem. Rev.* **2003**, *103*, 4419–4476; j) P. D. Beer, P. A. Gale, *Angew. Chem.* **2001**, *113*, 502–532; *Angew. Chem. Int. Ed.* **2001**, *40*, 486–516; k) J. Rebek, Jr., *Angew. Chem.* **2005**, *117*, 2104–2115; *Angew. Chem. Int. Ed.* **2005**, *44*, 2068–2078; l) M. Ruben, J. Rojo, F. J. Romero-Salguero, L. H. Uppadine, J-M. Lehn, *Angew. Chem.* **2004**, *116*, 3728–3747; *Angew. Chem. Int. Ed.* **2004**, *43*, 3644–3662; m) O. Lukin, F. Vögtle, *Angew. Chem.* **2005**, *117*, 1480–1501; *Angew. Chem. Int. Ed.* **2005**, *44*, 1456–1477; n) A. Chworos, I. Severcan, A. Y. Koyfman, P. Weinkam, E. Oroudjev, H. G. Hansma, L. Jaeger, *Science* **2004**, *306*, 2068–2072; o) A. Carbone, N. C. Seeman, *Proc. Natl. Acad. Sci. USA* **2002**, *99*, 12577–12582; p) N. C. Seeman, A. M. Belcher, *Proc. Natl. Acad. Sci. USA* **2002**, *99*, 6451–6455; q) N. C. Seeman, *Nature* **2003**, *421*, 427–431; N. C. Seeman, *Chem. Biol.* **2003**, *10*, 1151–1159; r) S. Liao, N. C. Seeman, *Science* **2004**, *306*, 2072–2074; s) H. Yan, *Science* **2004**, *306*, 2048–2049; t) B. Samori, G. Zuccheri, *Angew. Chem.* **2005**, *117*, 1190–1206; *Angew. Chem. Int. Ed.* **2005**, *44*, 1166–1181; u) K. V. Gothelf, R. S. Brown, *Chem. Eur. J.* **2005**, *11*, 1062–1069.

[3] a) G. Ashkenasy, R. Jegasia, M. Yadav, M. R. Ghadiri, *Proc. Natl. Acad. Sci. USA* **2004**, *101*, 10872–10877; b) G. Ashkenasy, M. R. Ghadiri, *J. Am. Chem. Soc.* **2004**, *126*, 11140–11141.

[4] a) D. S. Watts, S. H. Strogatz, *Nature* **1998**, *393*, 440–442; b) S. H. Strogatz, *Nature* **2001**, *410*, 268–276; c) H. Jeong, B. Tombor, R. Albert, Z. N. Oltval, A. L. Barabasi, *Nature* **2000**, *407*, 651–654; d) E. Ravasz, A. L. Somera, D. A. Mongru, Z. N. Oltvai, A. L. Barabasi, *Science* **2002**, *297*, 1551–1555; e) M. Girvan, M. E. J. Newman, *Proc. Natl. Acad. Sci. USA* **2002**, *99*, 7821–7826; f) R. Guimerà, L. A. N. Amaral, *Nature* **2005**, *433*, 895–900; g) J. J. Perez, *Chem. Soc. Rev.* **2005**, *34*, 143–152; h) K. Ding, H. Du, Y. Yuan, J. Long, *Chem. Eur. J.* 10, 2872–2884; i) R. R. Breaker, *Nature* **2004**, *432*, 838–845; j) C. M. Dobson, *Nature* **2004**, *432*, 824–828; k) J. J. Lavigne, E. V. Anslyn, *Angew. Chem.* **2001**, *113*, 3212–33225; *Angew. Chem. Int. Ed.* **2001**, *40*, 3118–3130.

[5] a) D. Philp, A. Robertson, *Chem. Commun.* **1998**, 879–880; b) C. A. Booth, D. Philp, *Tetrahedron Lett.* **1998**, *39*, 6987–6990; c) A. Robertson, D. Philp, N. Spencer, *Tetrahedron* **1999**, *55*, 11365; d) R. M. Bennes, B. M. Kariuki, K. D. M. Harris, D. Philp, N. Spencer, *Org. Lett.* **1999**, *1*, 1087–1090; e) R. M. Bennes, M. Sapro-Babiloni, W. C. Hayes, D. Philp, *Tetrahedron Lett.* **2001**, *42*, 2377–2380; f) S. J. Howell, D. Philp, N. Spencer, *Tetrahedron* **2001**, *57*, 4945–4949.

[6] a) L. J. Prins, D. N. Reinhoudt, P. Timmerman, *Angew. Chem.* **2001**, *113*, 2446–2492; *Angew. Chem. Int. Ed.* **2001**, *40*, 2382–2426; b) F. Diederich, P. J. Stang, *Template Directed Synthesis*, Wiley-VCH, Weinheim, **2000**; c) D. A. Moffet, M. H. Hecht, *Chem. Rev.* **2001**, *101*, 3191–3203; d) P. A. Brady, J. K. M. Sanders, *Chem. Soc. Rev.* **1997**, *26*, 327–336; e) D. Philp, J. F. Stoddart, *Angew. Chem.* **1996**, *108*, 1242–1286; *Angew. Chem. Int. Ed. Engl.* **1996**, *35*, 1154–1196; for applications see: C. Niemeyer, *Angew. Chem.* **2001**, *113*, 4254–4287; *Angew. Chem. Int. Ed.* **2001**, *40*, 4128–4158; J.-M. Lehn, *Chem. Eur. J.* **2000**, *6*, 2097–2102.

[7] a) S. P. Mathew, H. Iwamura, D. G. Blackmond, *Angew. Chem.* **2004**, *116*, 3379–3383; *Angew. Chem. Int. Ed.* **2004**, *43*, 3317–3321; b) D. G. Blackmond, *Proc. Natl. Acad. Sci. USA* **2004**, *101*, 5732–5736; c) F. G. Buono, H. Iwamura, D. G. Blackmond, *Angew. Chem.* **2004**, *116*, 2151–2155; d) K. Soai, T. Shibata, H. Morioka, K. Choji, *Nature* **1995**, *378*, 767–768; e) T. Shibata, K. Choji, T. Hayase, Y. Aizu, K. Soai, *Chem. Commun.* **1996**, 1235–1236; f) T. Shibata, H. Morioka, T. Hayase, K. Choji, K. Soai, *J. Am. Chem. Soc.* **1996**, *118*, 471–472.

[8] Some recent examples include: a) M. Kindermann, I. Stahl, M. Reimold, W. M. Pankau, G. von Kiedrowski, *Angew. Chem.* **2005**, *117*, 6908–6913; *Angew. Chem. Int. Ed.* **2005**, *44*, 6750–6755; b) R. Isaac, J. Chmielewski, *J. Am. Chem. Soc.* **2002**, *124*, 6808–6809; c) X. Li, J. Chmielewski, *J. Am. Chem. Soc.* **2003**, *125*, 11820–11821; d) X. Li, J. Chmielewski, *Org. Biomol. Chem.* **2003**, *1*, 901–904; e) S. Matsumura, T. Takahashi, A. Ueno, H Mihara, *Chem. Eur. J.* **2003**, *9*, 4829–4837; f) D. H. Lee, J. R. Granja, J. A. Martinez, K. Severin, M. R. Ghadiri, *Nature* **1996**, *382*, 525–528.

[9] For reviews, see: a) N. Paul, G. F. Joyce, *Curr. Opin. Chem. Biol.* **2004**, *8*, 634–649; b) X. Li, J. Chmielewski, *Org. Biomol. Chem.* **2003**, *1*, 901–904; c) R. Isaac, Y.-W. Ham, J. Chmielewski, *Curr. Opin. Struct. Biol.* **2001**, *11*, 458–463; d) A. Robertson, A. J. Sinclair, D. Philp, *Chem. Soc. Rev.* **2000**, *29*, 141–152; e) D. H. Lee, K. Severin, M. R. Ghadiri, *Curr. Opin. Chem. Biol.* **1997**, *1*, 491–496.

[10] a) G. von Kiedrowski, *Angew. Chem.* **1986**, *98*, 932–934; *Angew. Chem. Int. Ed. Engl.* **1986**, *25*, 932–935; b) G. von Kiedrowski, B. Wlotzka, J. Helbing, M. Matzan, S. Jordan, *Angew. Chem.* **1991**, *103*, 456–459; *Angew. Chem. Int. Ed. Engl.* **1991**, *30*, 423–426; c) B. G. Bag, G. von Kiedrowski, *Pure Appl. Chem.* **1996**, *68*, 2145–2152.

[11] a) D. J. Cram, *Angew. Chem.* **1988**, *100*, 1041–1052; *Angew. Chem. Int. Ed. Engl.* **1988**, *27*, 1009–1020; b) E. C. Constable, *Comprehensive Supramolecular Chemistry, Vol. 9* (Eds.: J. L. Atwood, J. E. D. Davis, D. D. Macnicol, F. Vögtle), Elsevier, New York, **1996**, pp. 218; c) S. J. Rowan, D. G. Hamilton, P. A. Brady, J. K. M. Sanders, *J. Am. Chem. Soc.* **1997**, *119*, 2578–2579; d) S. J. Rowan, J. K. M. Sanders, *J. Org. Chem.* **1998**, *63*, 1536–1546.

[12] For comprehensive kinetic analyses of minimal systems, see: a) G. von Kiedrowski, *Bioorganic Chemistry Frontiers, Vol.3*, Springer, Berlin, Heidelberg, **1993**, pp. 115–146; b) D. N. Reinhoudt, D. M. Rudkevich, F. de Jong, *J. Am. Chem. Soc.* **1996**, *118*, 6880–6889; c) F. M. Menger, A. V. Eliseev, N. A. Khanjin, M. J. Sherrod, *J. Org. Chem.* **1995**, *60*, 2870–2878.

[13] a) V. C. Allen, D. Philp, N. Spencer, *Org. Lett.* **2001**, *3*, 777–780; b) J. M. Quayle, A. M. Z. Slawin, D. Philp *Tetrahedron Lett.* **2002**, 43, 7229–7233.

[14] Efforts in other laboratories focused purely on rate acceleration via hydrogen-bonding recognition. We adopted cycloaddition reactions in the covalent bond-forming step since they simultaneously provide scope for the investigation of rate acceleration and the generation of selectivity, through monitoring the diastereoisomeric ratio, and are relatively immune to adventitious catalysis.

[15] a) J. D. Winkler, *Chem. Rev.* **1996**, *96*, 167–176; b) C. Cativiela, J. I. Garcia, J. A. Mayoral, L. Salvatella, *Chem. Soc. Rev.* **1996**, *25*, 209–218; c) H. B. Kagan, O. Riant, *Chem. Rev.* **1992**, *92*, 1007–1019.

[16] a) F. H. Allen, W. D. S. Motherwell, P. R. Raithby, G. P. Shields, R. Taylor, *New J. Chem.* **1999**, *23*, 25–34; b) J. Bernstein, R. E. Davis, L. Shimoni, N.-L. Chang, *Angew. Chem.* **1995**, *107*, 1689–1708; *Angew. Chem. Int. Ed. Engl.* **1995**, *34*, 1555–1573; c) M. C. Etter, *Acc. Chem. Res.* **1990**, *23*, 120–126; d) T. Steiner, *Acta Crystallogr. Sect. B* **2001**, *57*, 103–106; e) F. Garcia-Tellado, S. J. Geib, S. Goswami, A. D. Hamilton, *J. Am. Chem. Soc.* **1991**, *113*, 9265–9269; f) J. Geib, C. Vincent, E. Fan, A. D. Hamilton, *Angew. Chem.* **1993**, *105*, 83–85; *Angew. Chem. Int. Ed. Engl.* **1993**, *32*, 119–121; g) E. Fan., J. Yang, J. Geib, T. C. Stoner, M. D. Hopkins, A. D. Hamilton, *J. Chem. Soc. Chem. Commun.* **1995**, 1251–1252; h) B. König, O. Möller, P. Bubenitschek, *J. Org. Chem.* **1995**, *60*, 4291–4293; i) I. L. Karle, D. Ranganathan, V. Haridas, *J. Am. Chem. Soc.* **1997**, *119*, 2777–2783; j) C. Bielawski, Y.-S. Chen, P. Zhang, P.-J. Prest, J. S. Moore, *Chem. Commun.* **1998**, 1313–1314; k) N. Shan, A. D. Bond, W. Jones, *Tetrahedron Lett.* **2002**, *43*, 3101–3104.

[17] a) H. Kwart, K. King, *Chem. Rev.* **1968**, *68*, 415; b) P. J. Boul, P. Reutenauer, J.-M. Lehn, *Org. Lett.* **2005**, *7*, 15–18.

[18] a) J. R. McElhanon, D. R. Wheeler, *Org. Lett.* **2001**, *3*, 2681; b) X. M. Chen, A. Dam, K. Ono, A. Mal, H. Shen, S. R. Nutt, K. Sheran, F. Wudl, *Science* **2002**, *295*, 1698.

[19] SimFit, A program for kinetic simulation and fitting. D. Sievers, G. von Kiedrowski, *Chem. Eur. J.* **1998**, *4*, 629–641.

[20] The kinetic effective molarity is defined as the rate constant for the intracomplex reaction divided by the rate constant for the corresponding bimolecular reaction.

[21] The equilibrium or thermodynamic effective molarity is defined as the equilibrium constant for the intracomplex reaction divided by the equilibrium constant for the corresponding bimolecular reaction. In practice, this can be derived from the kinetic data by expressing the equilibrium constant (K_{eq}) as a ratio of the rate constants for the appropriate forward and reverse processes ($k_{forward}/k_{reverse}$).

[22] a) A. J. Kirby, *Adv. Phys. Org. Chem.* **1980**, *17*, 183–278; b) L. Mandolini, *Adv. Phys. Org. Chem.* **1986**, *22*, 1–111; c) R. Cacciapaglia, S. Di Stefano, L. Mandolini, *Acc. Chem. Res.* **2004**, *37*, 113–122.

[23] a) R. J. Pearson, E. Kassianidis, D. Philp, *Tetrahedron Lett.* **2004**, *45*, 4777–4780; b) R. J. Pearson, E. Kassianidis, A. M. Z. Slawin, D. Philp, *Org. Biomol. Chem.* **2004**, *2*, 3434–3441; c) E. Kassianidis, R. J. Pearson, D. Philp, *Org. Lett.* **2005**, *7*, 3833–3836; d) R. J. Pearson, E. Kassianidis, A. M. Z. Slawin, D. Philp, *Chem. Eur. J.* **2006**, *12*, 6829–6840.

[24] a) M. I. Page, W. P. Jencks *Proc. Natl. Acad. Sci. U. S. A.* **1971**, 68, 1678–1680; b) M. I. Page, *Philos. Trans. R. Soc. London Ser. B* **1991**, 332, 149–153.

[25] M. W. Schmidt, K. K. Baldridge, J. A. Boatz, S. T. Elbert, M. S. Gordon, J. H. Jensen, S. Koseki, N. Matsunaga, K. A. Nguyen, S. J. Su, T. L. Windus, M. Dupuis, J. A. Montgomery, *J. Comput. Chem.* **1993**, *14*, 1347–1363.

Received: April 3, 2006
Published online: September 1, 2006

